1-1-2017

Combustion Phasing Through Combustion Ionization In A Caterpillar C7 Compression Ignition Engine

Kamal Ashraf Assaad
Wayne State University,

COMBUSTION PHASING THROUGH COMBUSTION IONIZATION IN A CATERPILLAR C7 COMPRESSION IGNITION ENGINE

by

KAMAL ASSAAD

THESIS

Submitted to the Graduate School

of Wayne State University,

Detroit, Michigan

in partial fulfillment of the requirements

for the degree of

MASTER OF SCIENCE

2016

MAJOR: MECHANICAL ENGINEERING

Approved By:

_____

Advisor Date

DEDICATION

I dedicate my dissertation work to my family with a special feeling of gratitude to my loving parents and my infinitely loving wife without whom this thesis might not have been written. I am greatly indebted to you for your endless love, encouragement, and support. All I have and will accomplish are only possible due to your love and sacrifices.

ACKNOWLEDGEMENTS

To Dr. Naeim Henein, I want to express my sincere gratitude for your generous advice, guidance and encouragement throughout my research for this work. Your devotion and enthusiasm taught me how to successfully achieve goals. It is an honor for me to be your student.

To my colleagues Prasad Raut and Steven Zielinski, your friendship made the work enjoyable. Thank you for spending time and efforts studying and supporting each of the team members.

To Fadi Estefanous, thank you for your mentorship and help to start my professional career in the combustion engines field.

To Tamer Badawy, thank you for the guidance and being always ready to help and answering a lot of questions and doubts throughout the study.

To Sherif Matta, your Matlab, and electronic skills enlightened multiple ways for me to perform data analysis.

To Samuel Ayad, your support and friendship made this thesis work enjoyable. Thank you for having the time to listen, help and brainstorming.

To TARDEC team: Joseph Stempnik, Kevin Sharples and Brian Harbaugh, your knowledge and support helped to drive this research project to success.

To Tim Tappert and Marvin Bradley, thanks for spending numerous hours for machining parts with high accuracy on short notices.

TABLE OF CONTENTS

LIST OF FIGURES

CHAPTER 1.0: INTRODUCTION

The goal of this study is the use of ion current for the control of the start of combustion to achieve the goals of best fuel economy, peak power, and low soot emissions in a military engine.

To achieve the goals of military engines, there is a need to control the combustion process for different military fuels. An in-cylinder combustion sensor is required to achieve these goals.

There are two types of sensors that have been available for research and development over the last four decades, in-cylinder pressure transducers and ion current sensors.

Most of the effort has focused on the pressure transducer, however, up till now a pressure transducer suitable for use in production engines has not been developed yet, because of cost and durability concerns.

Ion current sensors have much smaller initial and maintenance cost compared to the in-cylinder pressure transducers. Also existing engine component can be used as an ion current sensor such as the glow plug in a diesel engine, the spark plug in a gasoline engine or the fuel injector in the two types of engines. In addition, ion current sensor does not need a special whole to fit it in the cylinder head.

The Main conceived disadvantage of using the ion current sensor is the Lack of reproducibility. Research at Wayne State University proved that the lack reproducibility of the ion current signal is directly related to lack of reproducibility of the combustion process and cylinder pressure signal.

In combustion engines, the average of hundreds of pressure signals is used to investigate the combustion process. Similarly, the average of hundreds of ion current signal can be used, however, a cycle by cycle analysis of the ion current signal can be used to investigate cycle to cycle variation in combustion.

CHAPTER 2.0: LITERATURE REVIEW

2.1 Chemi and thermal combustion ionization

Combustion of fuel/air charge in internal combustion engines is considered to be a complex process involving numerous different chemical reactions as the fuel itself is not a pure substance but it is a mixture of many different chemical compounds. Combustion ionization occurs when the temperature of the combustion chamber is high and energy released by the chemical reaction ionizes the reactant species in a chemical reactive combustible air-fuel mixture.

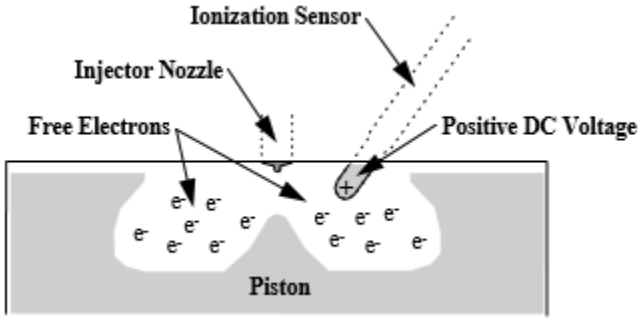

Figure 2. 1 Free electrons produced by ionized species [4]

Combustion ionization can be divided into two phases, Chemi-ionization, and thermal ionization. The most important chemi-ionization reactions in flames were noted as primary ionization reactions and found to be [4,5]

$$CH + O \rightarrow CHO^+ + e^- \quad (1)$$

$$CHO^+ + H_2O \rightarrow H_3O^+ + CO \quad (2)$$

With more H_3O^+ ions produced compared to CHO^+ ions since the reduction reaction (2) is faster than reaction (1). Glavmo et al [4] also presented the thermal ionization reaction in (3)

$$M + E_{ion} \rightarrow M^+ + e^- \quad (3)$$

Where M is a generic molecule, E_{ion} is the ionization energy, M^+ is the generic positive ion and e^- is the negative free electron.

The authors also stated that after a time period, depending on the reaction rate constants, electrons would recombine with the ions to form stable species. An example given by the authors of such a recombination reaction is

$$H_3O^+ + e^- \rightarrow H_2O + H \qquad (4)$$

Another reaction called 'electron deposit' reaction (5) was introduced by Kubach et al [5] to be added to reactions (1) and (2) as a primary reaction

$$C_nH_x + e^- \rightarrow C_nH_x{}^- \qquad (5)$$

Some additional reactions were stated by the authors as secondary ionization reactions (6) to (8)

$$CHO^+ + CH_2 \rightarrow CH_3{}^+ + CO \qquad (6)$$

$$O_2{}^- + C_nH_x \rightarrow C_nH_x{}^- + O_2 \qquad (7)$$

$$CH_3{}^+ + C_2H_2 \rightarrow C_3H_3{}^+ + H_2 \qquad (8)$$

And additional two recombination reactions, electron impingement (9) and dissociation (10).

$$A^+ + e^-{}_{ionized} + e^-{}_{imping} \rightarrow A + e^-{}_{imping} \qquad (9)$$

$$AB^+ + e^- \rightarrow A + B \qquad (10)$$

Henein et al [6] also presented (1) and (2) and added reaction (11) to the list of the primary reactions for ionization

$$CHO^+ + NO \rightarrow NO^+ + HCO \quad (11)$$

Also at rich and sooty hydrocarbon flames reaction (2) was substituted by reaction (12)

$$CH^+ + C_2H_2 \rightarrow {C_3H_3}^+ + e \quad (12)$$

The authors also found that that thermal ionization in high temperature combustion conditions mainly contributed by NO according to reaction (13)

$$NO + M \rightarrow NO^+ + e + M \quad (13)$$

Estefanous et al [7] listed reaction (14) to be added to the primary reaction (1) by Glavmo [4], reaction (15) and (16) to be added to reaction (2) as charge transfer reactions

$$CH + C_2H_2 \leftrightarrow {C_3H_3}^+ + e^- \quad (14)$$

$$CHO^+ + CH_2 \leftrightarrow {CH_3}^+ + CO \quad (15)$$

$$CHO^+ + NO \leftrightarrow NO^+ + CHO \quad (16)$$

While keeping reaction (17) as thermal ionization reaction

$$M \leftrightarrow M^+ + e^- \quad (17)$$

2.2 Ion Current measurement

2.2.1 Ion current probes

The basic principle of utilizing ion current sensors is installing a metal probe protruding inside the combustion chamber and electrically insulated from engine body supplied with a DC voltage source. With no combustion events occurring, the DC circuit is open and no current flows. However, when combustion occurs, current flows as the free electrons are attracted to positive DC voltage applied to the ion current sensor. Figure (2.2) shows the basic principle ionization circuit.

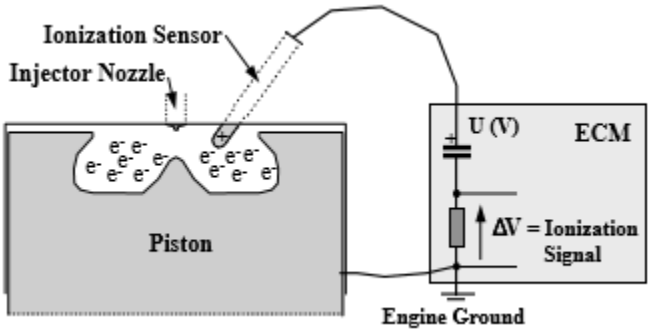

Figure 2. 2 Ionization circuit diagram of ion current probe [4]

Ion current is calculated by measuring the voltage across a known resistor divided by the resistor value. Glavmo et al. [4] also showed the ion current sensor probe design used in their experiments. The design incorporates a steel conductor electrically insulated from a steel shell fixed in the cylinder head by ceramic rings as shown in figure (2.3)

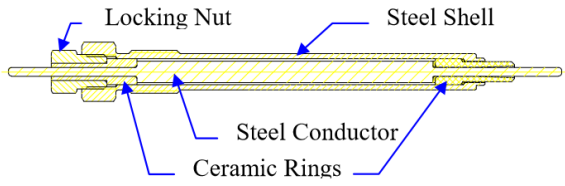

Figure 2. 3 Ionization sensor probe [4]

Glavmo et al. [4] successfully tested the ionization sensing technology in detection of pilot and main combustion events at same running conditions with different injection timings.

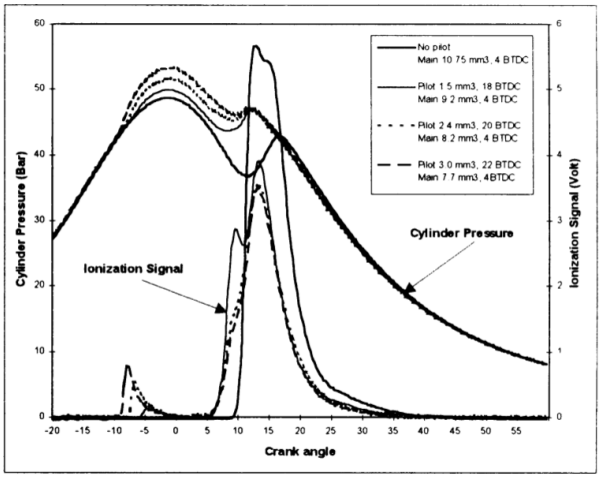

Figure 2. 4 Pilot and main combustion events detection by ionization sensing [4]

2.2.2 Glow plug ion current sensors

One drawback of using probes for ion current measurement is soot accumulation. In heavy duty diesel engines, soot is produced heavily and accumulates on the ion current sensing probe till the soot accumulated is in touch with the engine body and electrical insulation is compromised.

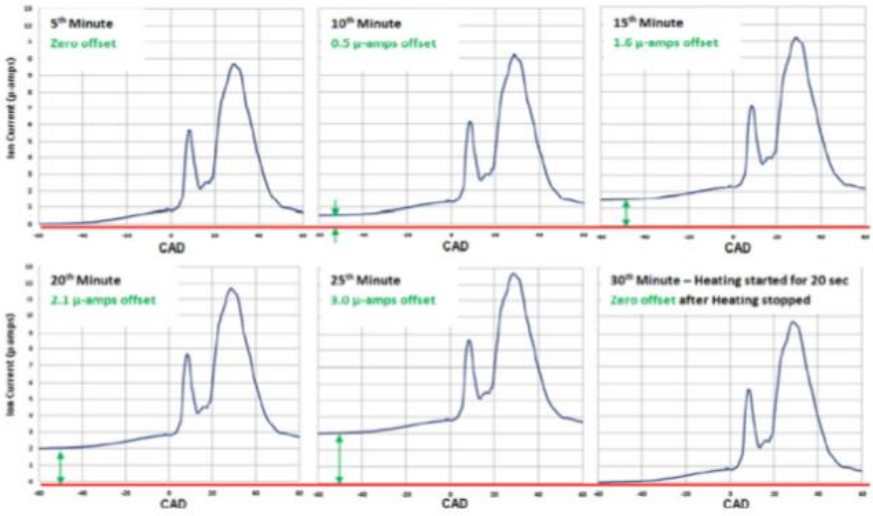

Figure 2. 5 Offset in ion current signal due to soot accumulation [6]

Researchers at Wayne State University developed a glow plug ion current sensor to overcome the drawback of using a simple ion probe by applying ceramic coating the inner central electrode and heater of a glow plug [8]. Figure (2.6) shows the construction of the modified glow plug ion sensor.

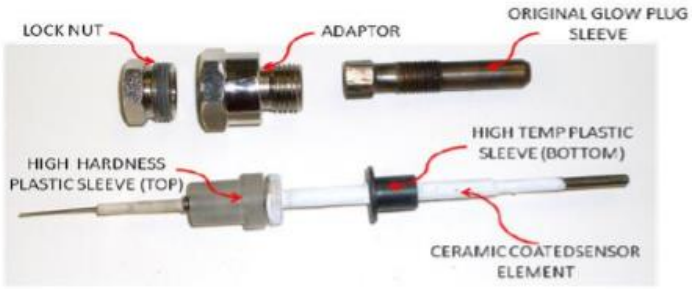

Figure 2. 6 Modified glow plug ion sensor [8]

A more advanced ionization circuit shown in figure (2.7) is required to support two functions. The first is ion current sensing and the second function is glow plug activation for cold starting conditions and if Soot is accumulated on the glow plug sensing tip to retrieve ion sensing functionality.

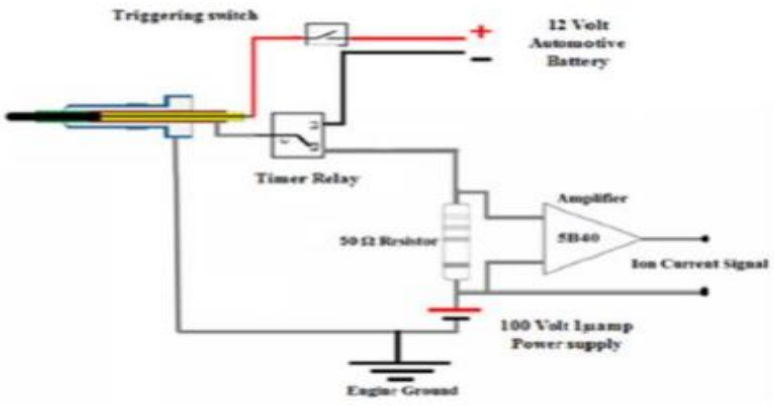

Figure 2. 7 Advanced glow plug ionization circuit [2]

Estefanous et al [3] developed a multi sensing fuel injector (MSFI) for ion current sensing of direct injected engines that are not equipped with glow plugs.

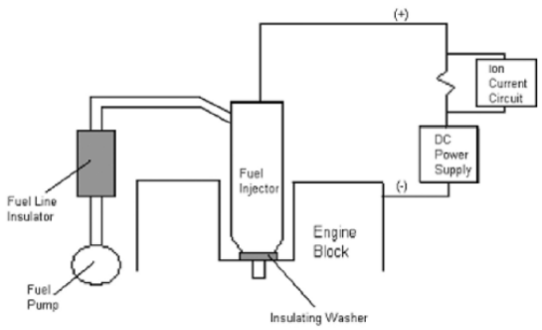

Figure 2. 8 Multi sensing fuel injector [3]

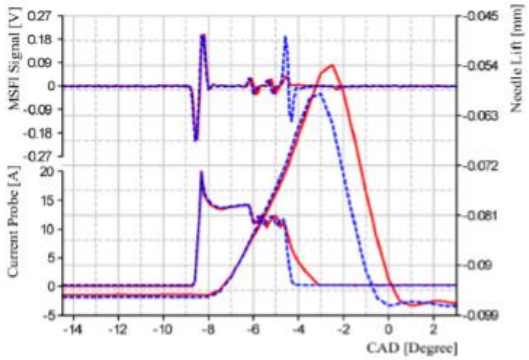

Figure 2. 9 Injection malfunction detection using MSFI [3]

With the new type of ion sensor, the authors were able to detect injector malfunction through combustion ionization. Figure (2.9) shows the benefit of using the injector as an ion current sensor. Shown in the figure the injector current, needle lift signal and ion current signal from the injector. The blue lines represent a healthy injection event when lines in red represent the injector malfunction. Ion current signal successfully detected the energizing and de-energizing currents of the injector and needle malfunction.

2.2.3 Ion current sensor location

For SI engines, ion current sensor location is critical as Peron et al [9] proved in their paper that if the ion current sensor is far from the spark plug location, it is fairly hard to distinguish between flame from and post flame front events. In case of CI engines, the charge is heterogeneous and start of combustion location changes within the cycle to cycle variations or even combustion can take place in several places at the same time.

Kubach et al [5] studied the effect of sensor location on the characteristics of the ion current signal by placing 4 different ion sensing probes inside a single cylinder. Figure (2.10) shows the different location of the ion sensors.

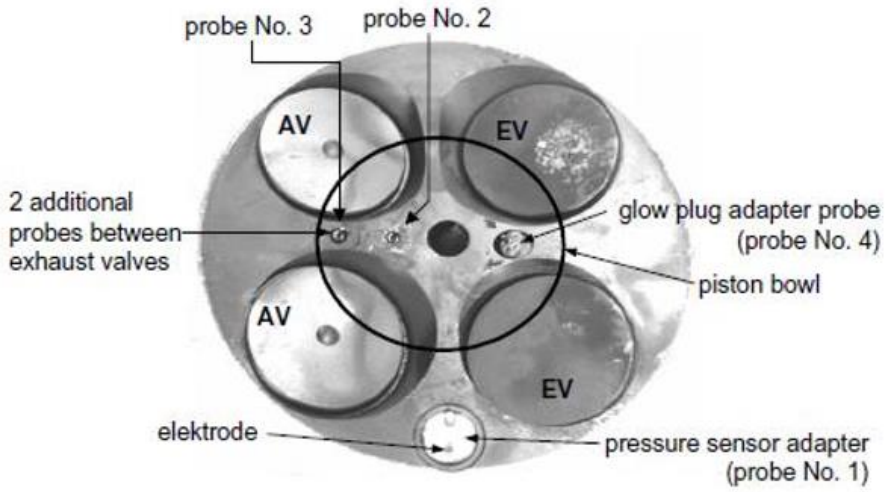

Figure 2. 10 Effect of ion sensor location on signal characteristics [5]

Through experiments it was concluded that best ion current sensor location is close to the fuel injector and far from the location with high levels of soot formation.

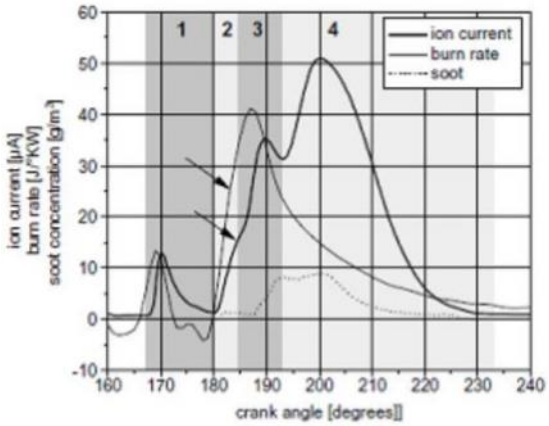

Figure 2. 11 Typical ion current signal from a CI engine with pilot injection [5]

Badawy et al [20] controlled the start of injection event of a common rail compression ignition engine by using the ion current as a feedback signal to the engine control unit at steady state and transient operating conditions based on a correlation between the start of ion current signal and the location of peak premixed combustion from the rate of heat released analysis.

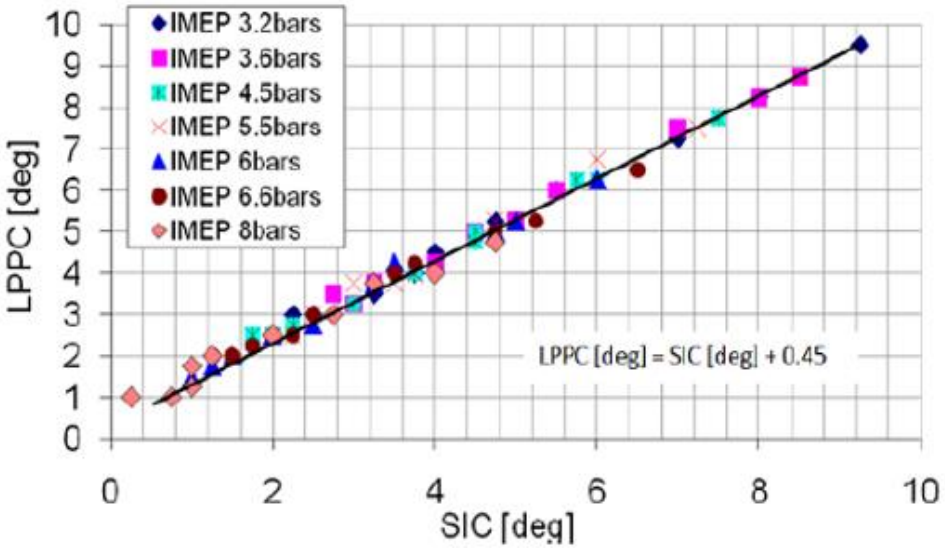

Figure 2. 12 SIC and LPPC correlation [20]

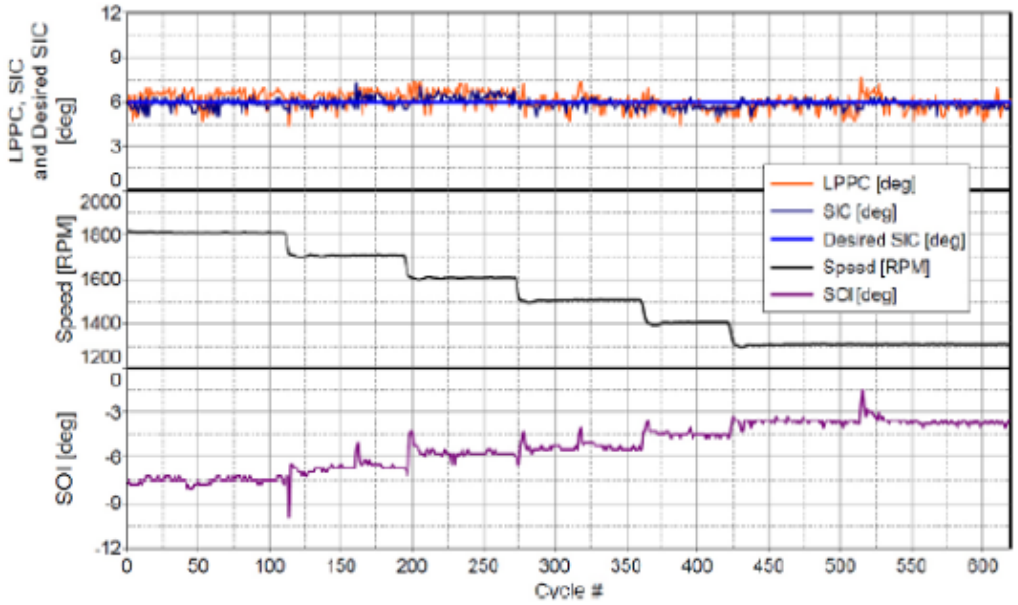

Figure 2. 13 Using ion current as a feedback signal for engine control [20]

2.2.4 Ion sensor tip shape

Henein et al [6], proved that increasing the surface area of the ion sensor exposed to the combustion results in increasing the amplitude of the ion current data as it averages the data collected over the depth of penetration into the combustion chamber. However, using a short length of ion sensor tip achieves more detailed data of ion current signal.

Larsson et al. [21] studied the effects of exposed surface area and protrusion into the combustion chamber on the ion current signal and agreed with Henein et al [6]. The authors also studied the effect of the shape of the sensor tip and concluded that at same surface area shape does not have a significant effect on the ion current signal.

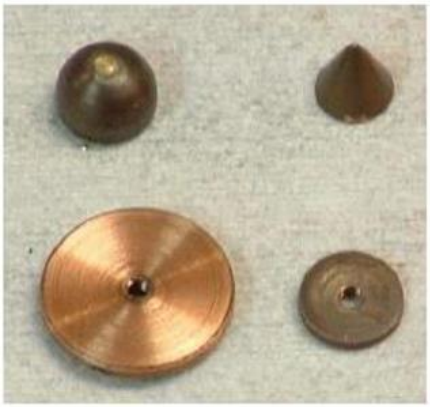

Figure 2. 14 Effect of sensor tip shape on ion current signal [21]

CHAPTER 3.0: EXPERIMENTAL SETUP

3.1 Engine

A six in-line cylinders water-cooled turbocharged Caterpillar C7 ACERT (Advanced Combustion Emission Reduction Technology) engine was used in this research project equipped with HEUI (Hydraulic Electronically Controlled Injection System) direct injection system as Caterpillar C7 engines are widely used in military vehicles, heavy-duty off-road trucks, and construction equipment.

Figure 3. 1 Caterpillar C7 engine and dynamometer setup

Engine	Caterpillar C7 ACERT
No. of Cylinder / Cylinder arrangement	6 / inline
Displacement	7.24 L
Compression Ratio	16.5:1
Firing Order	1-5-3-6-2-4
Bore and Stroke	110mm X 127mm
Injection System	HEUI-B Direct Injection
Peak Torque	1166 N-m @ 1440 rpm
Peak Power	246 kW @ 2395 rpm

Table (3.1) Caterpillar C7 engine specifications

3.2 Dynamometer

The C7 engine was mounted on a cart and connected by a flexible joint to a Froude-Hofmann 480 VAC, 3 phase dynamometer. This dynamometer is capable of loading up to 350 KW and supports manual and automatic test procedures. AC dynamometers are known for their fast response and accurate loading with the ability to perform various testing cycles such as FTP (Federal Test Procedure) cycle. The dynamometer along with high-speed IGBT (Insulated Gate Bipolar Transistor) and precise control algorithm provides transient and steady state control through a Texcell V12 software interface.

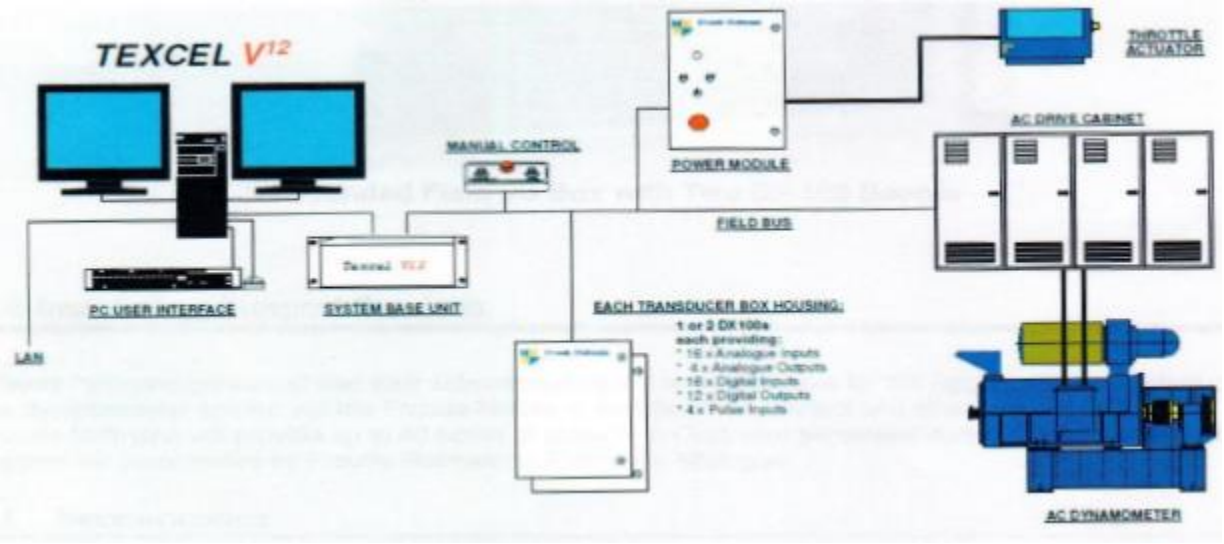

Figure 3. 2 Froude Hofmann 480 AC dynamometer setup

3.3 Cylinder head modifications

Caterpillar C7 engine does not utilize glow plugs however, an air heater is installed in the air intake manifold of the engine for cold starting purposes. Since no glow plug bore can be utilized for instrumenting in-cylinder sensors, drilling two bores was required to accommodate the in-cylinder pressure transducer and the ion current sensor.

Caterpillar Inc. provided a suitable location for the in-cylinder pressure transducer parallel to the injector. Choosing the second bore location was a challenge since ion current sensing is greatly affected by the sensor location. The ion sensor is required to protrude inside the combustion chamber to have more surface area for ionization measurements. If the ion sensor is installed in a way where the sensor tip can be wetted by the injection spray, engine performance would be affected as the fuel wetting a wall would not participate in the combustion process because of the low temperature of the wall. In addition, ion current measurement would not be possible.

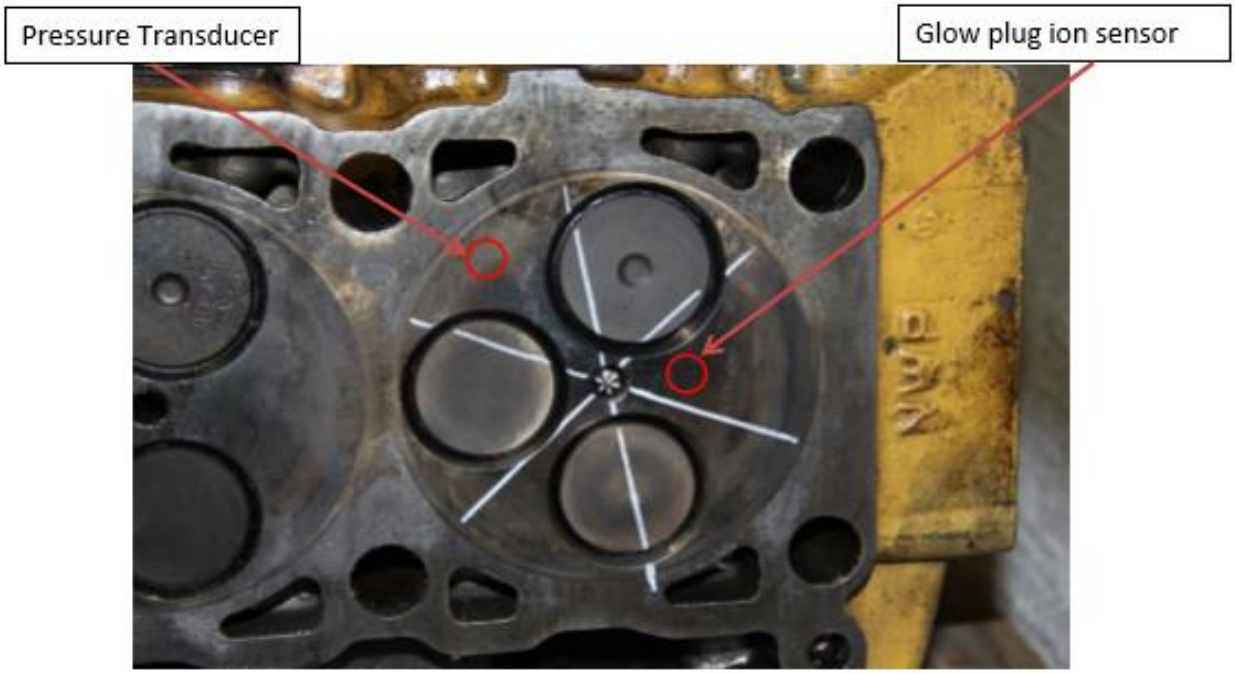

Figure 3. 3 Bottom view of selected sensor location in engine cylinder head

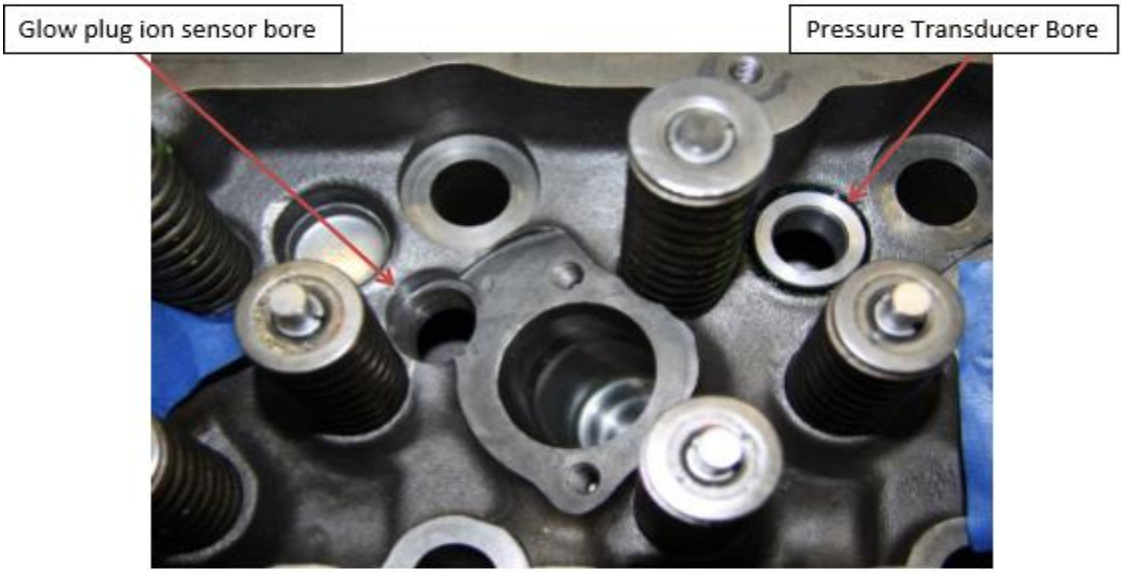

Figure 3. 4 Top view of selected sensor location in engine cylinder head

It was decided later to switch the sensors locations to be utilized as shown in figures (3.3) and (3.4) in order to avoid obstructing the piston movement by the protruding ion sensor. It is safer to use the first location for the ion sensor as the protruding tip would be located within the piston bowl area while the pressure sensor would be flush mounted to the firing deck away from the piston top surface. A 3d model shown in figure (3.5) was sketched in order to visualize the sensors locations with the piston at TDC.

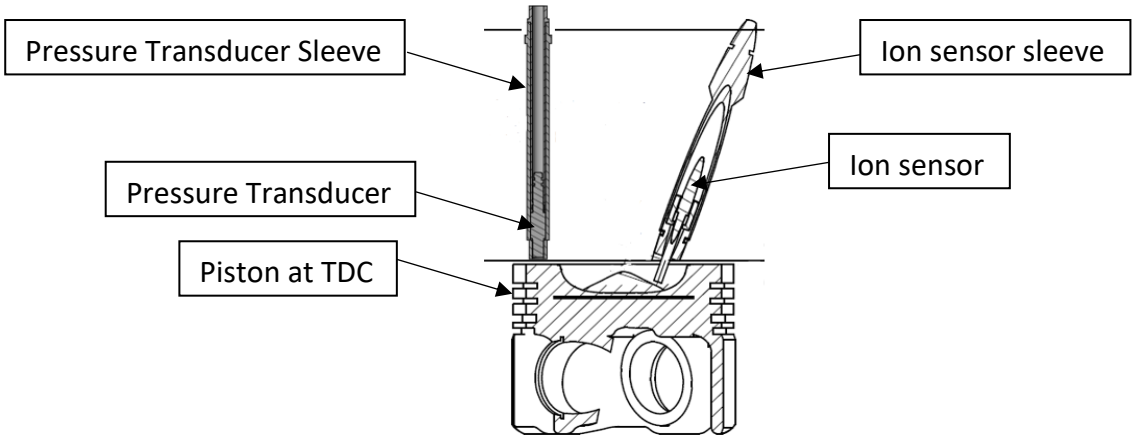

Figure 3. 5 Illustration of in-cylinder sensors locations

3.4 Data Acquisition System

Two data acquisition systems were used in this research synchronized by cycle number.

1	**Kistler Kibox Togo** High-speed data acquisition system
2	**ETAS ES600 module** Low-speed data acquisition system
3	**Ion box**
4	**ETAS 400 modules** Analogue to digital modules
5	**Kistler in-cylinder pressure transducer**
6	**Ion probe**
7	**Pressure transducers**
8	**Thermocouples**
9	**CAT C7 engine**
10	**Optical crankshaft encoder**
11	**Shell and Tube heat exchanger**
12	**Fuel cart**
13	**Three-way control valve**

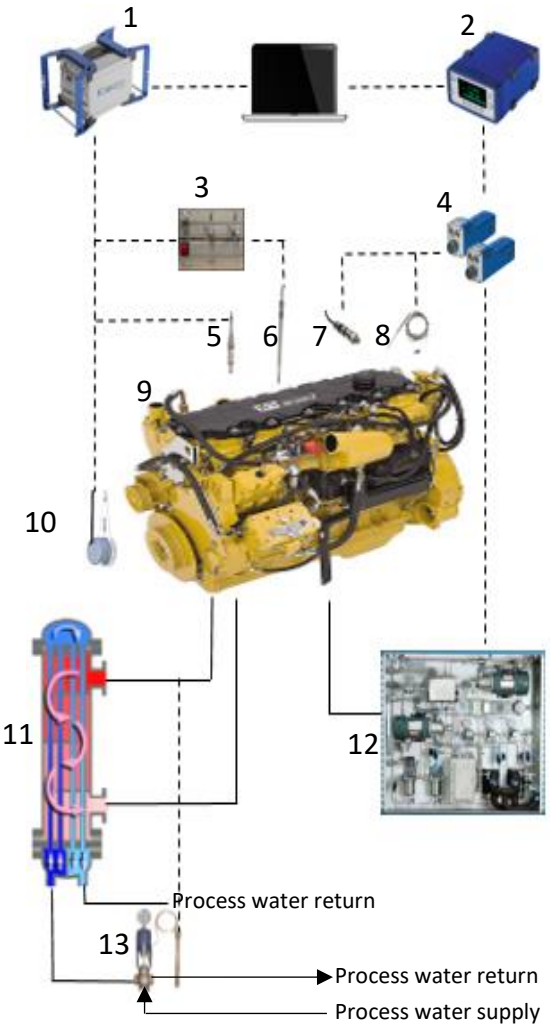

Figure 3. 6 Engine instrumentation and data acquisition systems

3.4.1 Low-speed data acquisition

ETAS daisy chain data acquisition system was used to collect low-speed data of test cell and engine temperatures, pressures and flow meter sensors.

To measure pressure parameters across the engine, Kulite pressure transducers were used with a range of (0-50 PSI). Exhaust temperatures were measured using K-type thermocouples due to the high measurement range. J-type thermocouples were used to measure cooling fluid and oil temperatures. A Pierburg PII 404 fuel cart was used to filter, supply and measure fuel density and consumption. Yokogawa flow meters were installed to the engine coolant lines and cooling process water lines to calculate heat loss data. A shell and tube heat exchanger was installed to circulate engine coolant in one loop and cooling process water provided from a cooling tower in the other loop. In order to have precise control over the coolant temperature, a self-acting three-way control valve was installed to the cooling water loop with the temperature sensor connected to the engine coolant out port. The control valve has a bulb containing a gas that expands or retracts according to the sensed temperature. The pressurized gas acts on a seat restricting the flow of the cooling process water to have it either bypass the heat exchanger if the coolant temperature is less than the set temperature or pass through the heat exchanger in case coolant temperature is higher than the set temperature. Figure (3.7) shows the operation of the three-way self-acting temperature control valve.

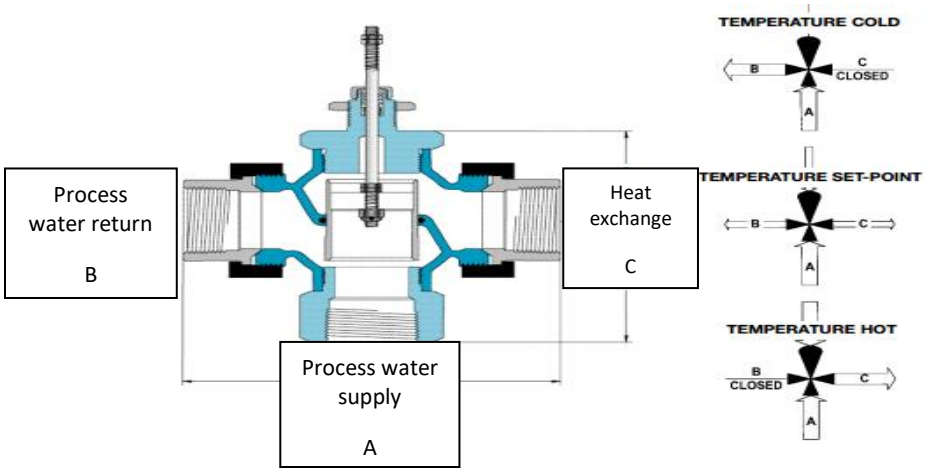

Figure 3. 7 Three-way self-acting temperature controlled valve for engine coolant

3.4.2 High-speed data acquisition

A Kistler Kibox Togo combustion analyzer was used to collect in-cylinder pressure signal from a Kistler 6125C piezoelectric pressure transducer which is able to measure pressures up to 300 Bars accurately at high temperatures and calculate the rate of heat released and integrated rate of heat released using the first law of thermodynamics neglecting heat losses to the walls. The pressure transducer was installed in a sleeve as the sleeve goes through the cooling fluid jackets of the cylinder head. Figures (3.8) shows respectively the pressure transducer used and the sleeve machined to accommodate the pressure transducer in cylinder 5 of the engine.

Figure 3. 8 In-cylinder pressure transducer and pressure sleeve

Also, a high-speed current clamp was connected to the high-speed data acquisition system to capture the injection current command pulse to determine the start and end of injection commands and the injection duration.

To synchronize data and record different high-speed combustion parameters, a Kistler optical crank angle encoder was connected to the Kibox with a 0.5 crank angle degree resolution. Also, Kibox software is capable of achieving better resolution of 0.1 crank angle degrees by interpolation between points. Top dead center was determined by the software from measuring the motoring cylinder pressure and heat loss angle of 1 CAD given by the engine supplier.

An ion amplifier box was connected to the ion current sensor instrumented in cylinder 5 of the engine. The ion box applies 100 VDC to the ion sensor. When combustion occurs, the circuit is completed by attracting the free electrons by the ionized species and electrical current starts flowing through a known resistance. Ion current is calculated by dividing the measured voltage across the ion box resistance by the resistance value. The ion box was connected to the high-speed data acquisition system to measure ion current signal against the crank angle degree with

high resolution to correlate the ion signal with other combustion parameters. Figure (3.9) explains the circuit diagram of the ion box [4].

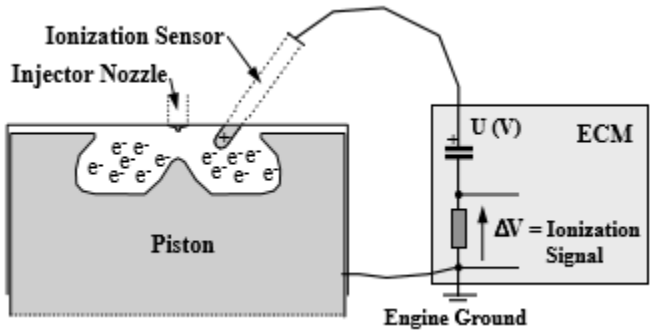

Figure 3. 9 Ionization circuit diagram [4]

Ion current sensor was integrated into a sleeve and electrically insulated from engine body by insulating bushings. Figure (3.10) shows the assembly of the ion sensor probe design integrated into the sleeve.

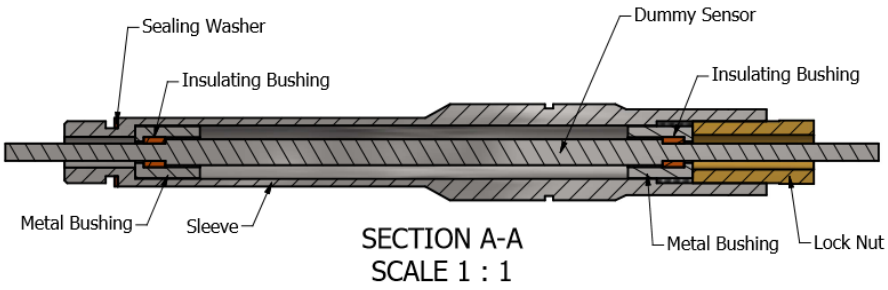

Figure 3. 10 Caterpillar C7 ion current probe design

Various materials were tested for fabricating the insulating bushings. Ceramic alumina material was tested as it withstands up to 2000 DegF but usually breaks when applying 10 Nm torque on the locking nut. After various attempts to insulate the ion current sensor, high-temperature PEEK 1000 was used to fabricate the insulating bushings which can be replaced easily after certain hours of operation or depending on the ion signal integrity. High-temperature heat shrink was also used to electrically insulate the ion probe from the metal bushings.

The metal bushings were crucial parts of the design as they serve as heat shields for the insulating bushings not to melt and find its way into the combustion chamber and also to distribute the tightening load evenly over the whole contact area on the insulating bushings.

Figure 3. 11 Caterpillar C7 ion sensor sleeve.

CHAPTER 4.0: EXPIREMENTAL DATA AND ANALYSIS

4.1 Introduction to HEUI injection systems

In order to meet the stringent emissions regulation and EPA requirements while preserving the engine performance, output power, and fuel economy, Caterpillar and Navistar established a partnership in 1987 to develop a new injection system for direct injection compression ignition engines.

The HEUI injection system can achieve a maximum of 180 MPa injection pressure with the capability of injection rate shaping and multiple injection events to achieve better performance independent of engine speed and with no mechanical actuation required for injection timing. This puts the HEUI injection systems in a top-ranked rating compared to the preceding unit injection systems designs.

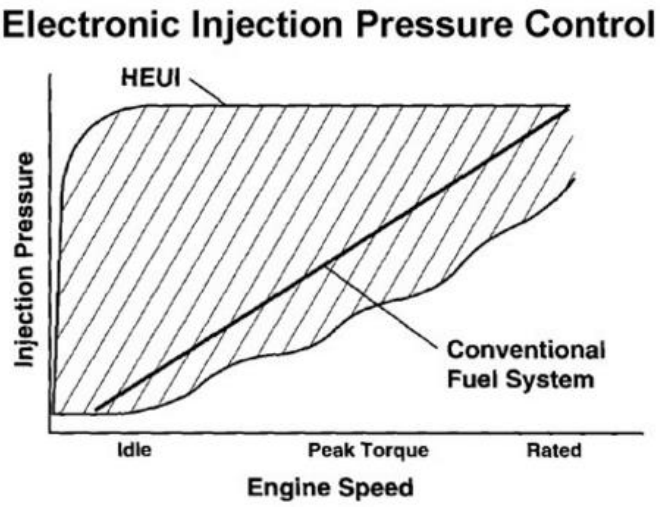

Figure 4. 1 HEUI injection pressure control [11]

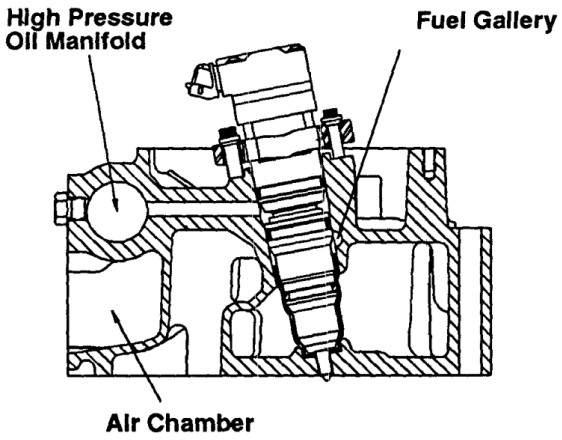

Figure 4. 2 Cylinder Head Showing oil and fuel port to HEUI [12]

Figure (4.2) shows the cross section of a cylinder head with high pressure oil manifold for injection actuation oil transferred by a high pressure oil pump (Typically 230 bars pressure). Another gallery in the cylinder head is made to deliver fuel to the injector at a lower pressure (2 bars).

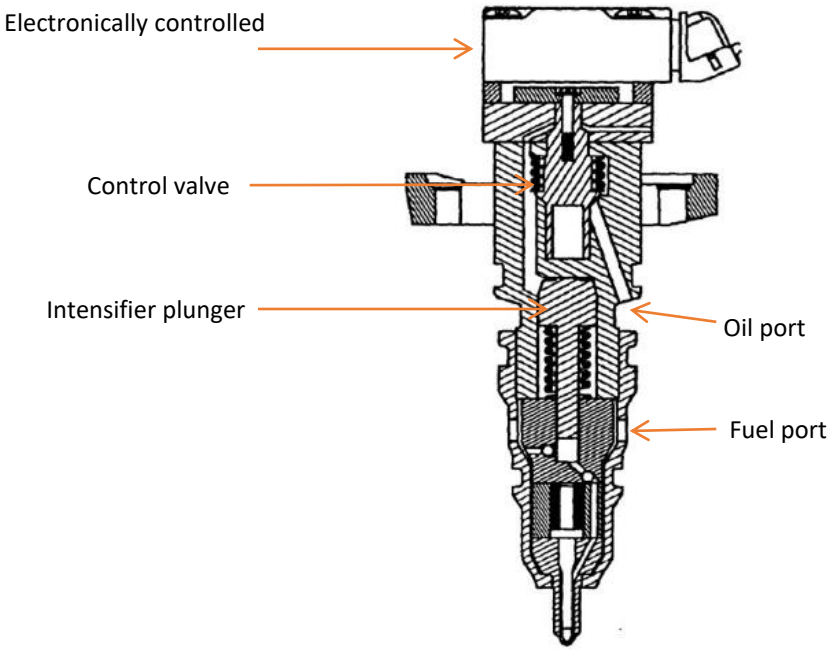

Figure 4. 3 Cross section view of Caterpillar HEUI injector [12]

When an electronic injection waveform is supplied to the solenoid, the control valve is opened allowing the pressurized oil transferred through the oil gallery to travel through the injector and act on the intensifier plunger to pressurize the fuel according to an area ratio in the plunger geometry between the oil and fuel. This area ratio has been reported to be 7:1 [12]. Once the pressure exceeds spring forces, the needle lifts and injection starts.

One of the key features of the HEUI injection systems is the ability to apply rate shaping to the fuel injection to optimize engine performance and meet emissions standards.

Figure (4.4) shows an injector current supplied to injector solenoid with a pull in peak current to aggressively pull in the control valve followed by a holding current to hold the control valve in the opening position allowing oil to pressurize the fuel. Also shown the poppet lift and the injection rate resulted from the injection current.

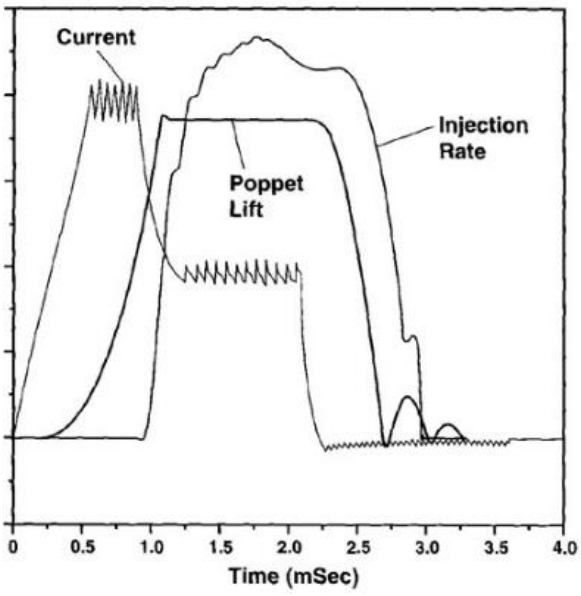

Figure 4. 4 Injection command, Poppet lift response and Injection rate [11]

4.2 Caterpillar HEUI-B

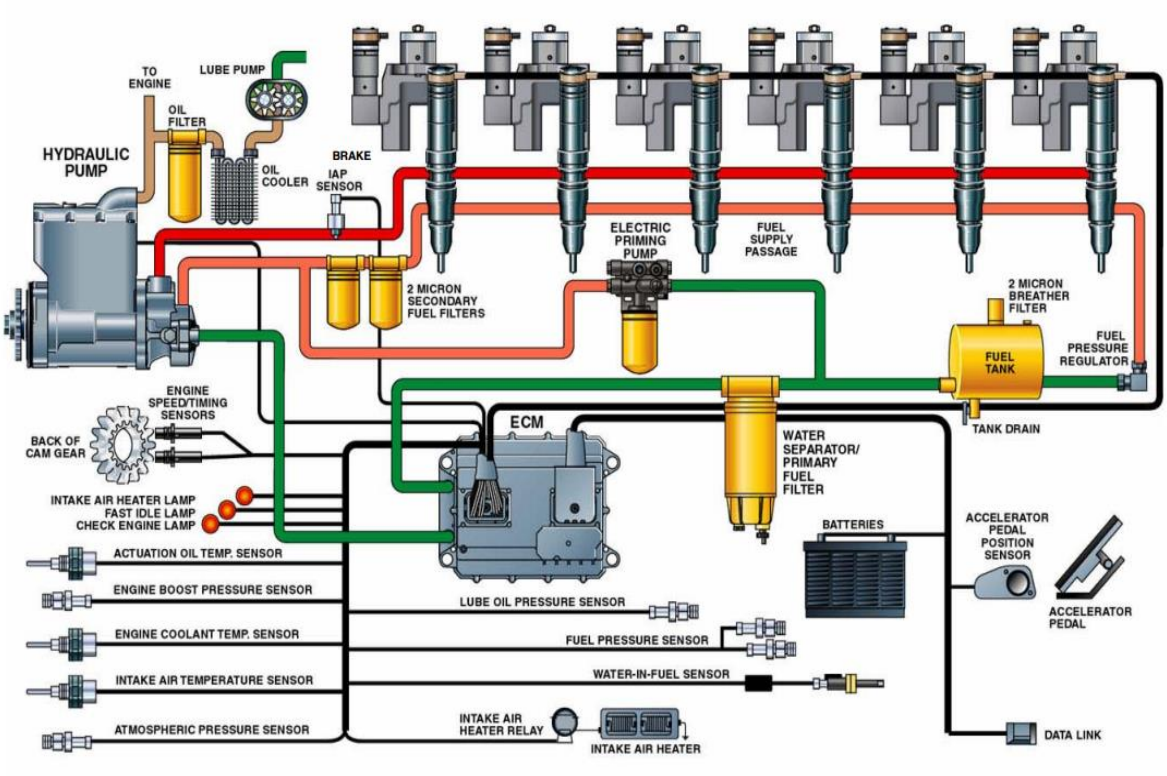

Figure 4. 5 Caterpillar HEUI-B system schematic [13]

In 2003, Caterpillar published a paper describing a newer version of HEUI injectors. The HEUI B system is the same as preceding HEUI systems with some extra enhancements to the mechanical parts of the injector to improve the rate shaping capabilities and have lower pressure drops in the fluid systems.

Figure (4.5) shows the schematic of the HEUI-B system components. A gear pump delivers engine oil from the oil sump to the high pressure oil pump. The high pressure oil flows through the oil gallery in the engine cylinder head to the injectors at around 280 bars pressure. Fuel travels from the fuel tank by a fuel pump operated by the high pressure hydraulic pump to the fuel gallery in

the engine cylinder head that acts as a fuel common rail but at a much lower pressure of about 5 to 7 bars. Figure (4.6) shows a detailed cross section of the HEUI-B injector by Caterpillar.

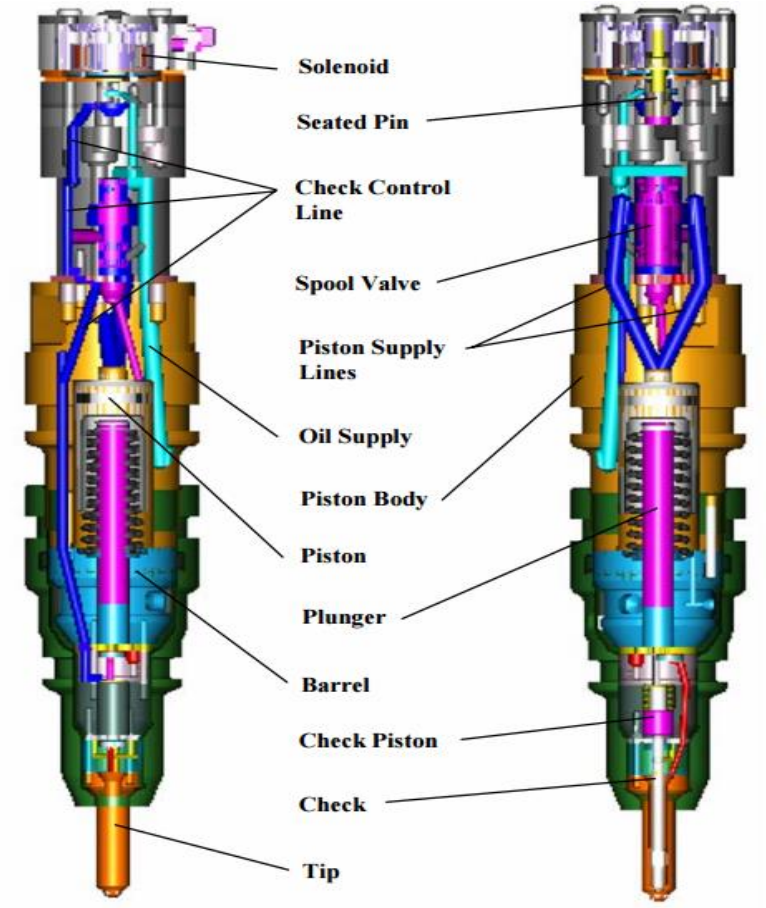

Figure 4. 6 Caterpillar HEUI-B cross section view [13]

In HEUI-B, High pressure oil is not only acting on the intensifier when the solenoid is energized to start injection but also acting on the check piston when the solenoid is de-energized to close the nozzle at the end of injection.

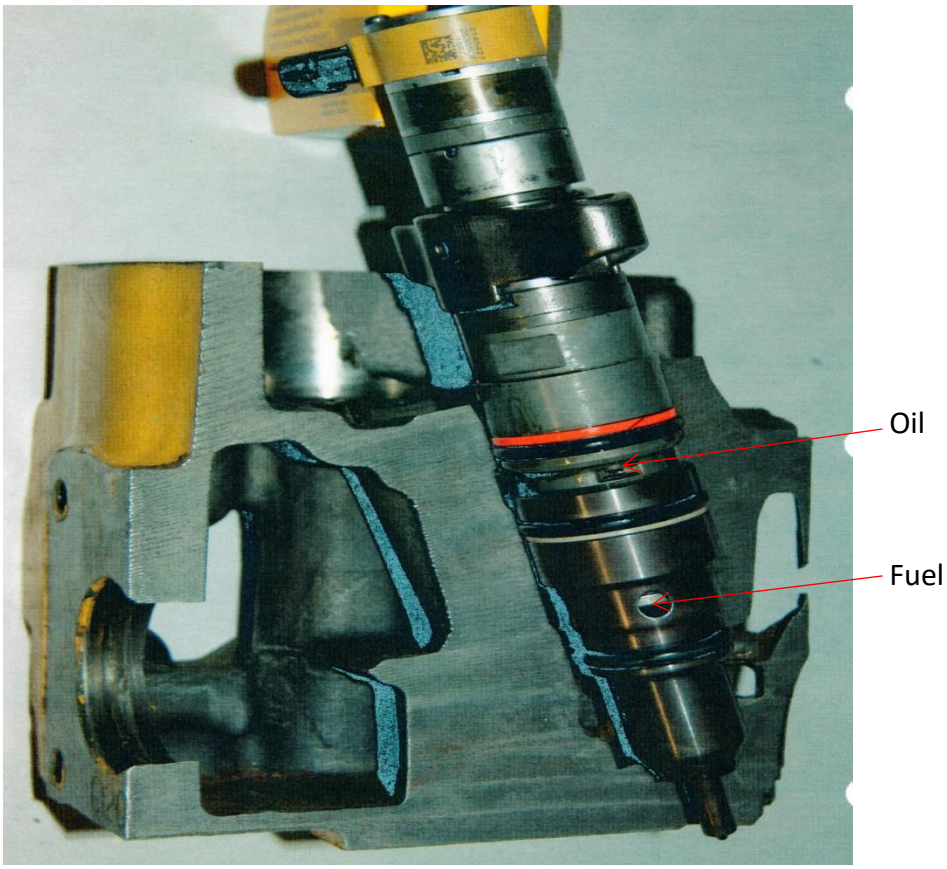

Figure 4. 7 Caterpillar C7 HEUI-B Injector

4.3 Single ramp profile main injection

4.3.1 HEUI injector operation

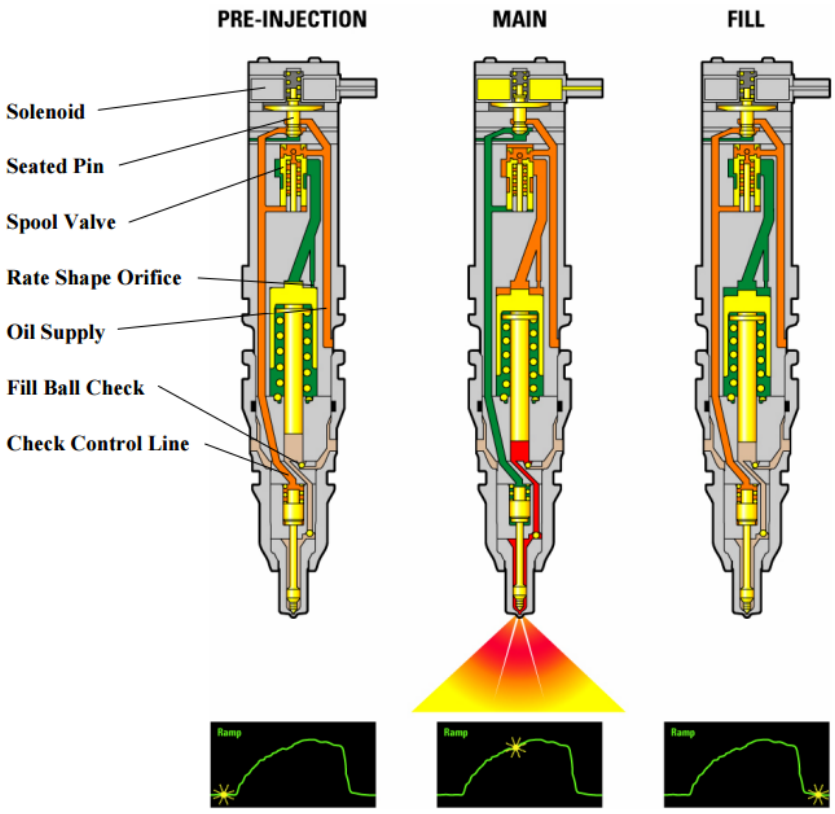

Figure 4. 8 HEUI-B Single ramp injection [13]

In order to obtain a single injection with the ramp profile, a single current waveform is provided to the solenoid. A single injection with a ramp profile can be summarized in three stages as shown in figure (4.8):

A- **Pre-injection:** High pressure oil travels through the injector body acting on the check piston to keep the needle closed before injection events. In this stage, the seated pin is preventing the pressurized oil to act on the intensifier piston.

B- **Main Injection:** The seated pin is pulled when the solenoid is energized by a single current waveform from the injection driver embedded in the engine control unit. This motion of the seated pin allows the oil to start accumulating at the intensifier plunger cavity pressurizing the plunger causing it to move downwards to pressurize the fuel according to the intensification ratio. Also, the motion of the seated pin allows evacuating the pressure acting on the bottom check piston creating a greater pressure difference on the needle springs when the high pressure fuel arrives at the needle causing the needle to lift and start the injection delivery to the combustion chamber. During the main injection event, the movement of the plunger downwards pressurizing the fuel causes the fill ball check to block the fuel port for pressure build up.

C- **Fill:** At the end of the injection event, the solenoid valve is de-energized causing the seated pin to move downwards allowing the high pressure oil to push the check piston downwards closing the needle and also acting on the bottom of the spool valve to prevent the oil from pressurizing the intensifier plunger.

At the start of the main injection stage, high pressure oil is acting on the intensifier plunger while it is seated on its upper seat through the rate shape orifice resulting in an initially slow rate due to the small force. Once the intensifier plunger disengages from its upper seat, the pressure and rate start climbing dramatically leading to a ramp injection profile.

4.3.2 Start of fuel delivery and start of combustion analysis

Due to the complexity of the HEUI injection system, it is justified to define an injection delay period as the difference in crank angle degrees between the start of injection pulse to the start of fuel delivery since actuation oil takes time to travel through the injector and apply actuation pressure on the mechanically moving parts of the injector.

HEUI injectors from Caterpillar are always accompanied by CDs (Compact disks) containing trim files to be programmed to the ECU before running the engine on new injectors to allow the engine to run smoothly with less harmful exhaust emissions to the environment. Trim files are generated because the behavior of the mechanical parts of different injectors is not the same for each injector. Each injector is tested after assembly to measure the injection delay time at different engine operating conditions.

Since a needle lift sensor was not available, another study is performed to come up with start of fuel delivery event through the calculated apparent rate of heat released.

Apparent rate of heat released is calculated from the first law of thermodynamics neglecting the heat transfer to the walls of the combustion chamber using:

$$\frac{dQ}{d\theta} = \frac{n}{n-1} P \frac{dV}{d\theta} + \frac{1}{n-1} V \frac{dP}{d\theta} \qquad (18)$$

Where n is the polytropic coefficient index.

P is the cylinder pressure.

V is the calculated volume at each crank angle degree.

A constant average n of 1.344 was calculated for all the test runs to be able to compare the apparent rate of heat released curves of different operating conditions.

To study the characteristics of the HEUI injector with a single injection event and a ramp injection profile, a 500 Ohms resistor is connected across the terminals of the coolant temperature sensor to force the engine control unit to apply the cold calibration tables utilizing single ramp profile injection.

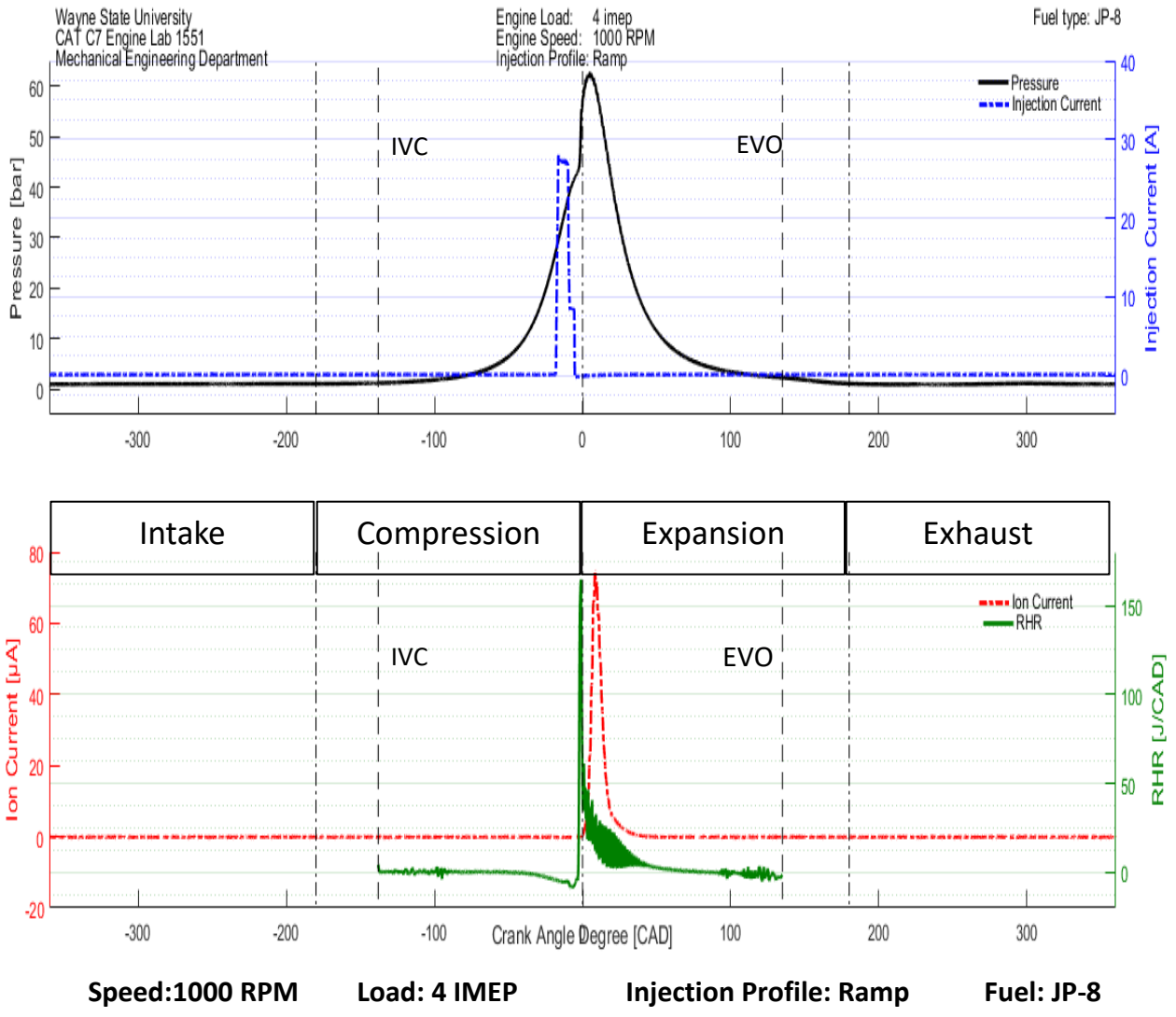

Figure 4. 9 Sample data at 1000RPM 4IMEP Ramp injection

Figure (4.9) illustrates the measured and calculated signals to study injection and combustion parameters of the HEUI injection systems over an average of 100 cycles. Pressure trace records a gradual increase due to the compression stroke of the air followed by a sharp increase slightly after the fuel injection pulse due to the auto-ignition of the air-fuel mixture. As a result of gasses expansion, pressure starts decreasing till the exhaust valve opens at EVO (Exhaust Valve Opening) event for an exhaust blow out period evacuating the combustion chamber leaving the engine ready for a fresh charge.

Also shown in the figure apparent rate of heat released by the fuel to the system. Signals calculated from IVC to EVO. In addition to ion current signal recording a peak due to the exothermic reactions and combustion of the air-fuel mixture.

Illustrated in figure (4.10) the rate of heat released curve calculated with the average of 100 cycles against the injection current waveform having the engine operated at cold mode to obtain the single ramp injection rate profile at 1000 rpm light load (4 IMEP). Start of main injection event is represented by SOIP (Start of Injection Pulse) throughout the study. SOIP is defined to be the location in CAD when the injection current signal exceeds a chosen threshold of 0.75A.

Start of injection pulse (SOIP) at 17.9 CAD bTDC is followed by a sharper decrease in the rate of heat released trace representing the actual start of fuel delivery (SOFD) at 10 CAD bTDC as the fuel injected is at a much lower temperature compared to the compressed air inside the combustion chamber causing heat to be absorbed by the fuel from the surrounding system having an injection delay of 7.9 CAD.

Researchers used different definitions to define the SOC (Start of Combustion) of the main charge. In this study, SOC is defined as the location in CAD where the rate of heat release trace shows a rise indicating that a huge amount of heat released by the combustion of the fuel/air mixture to the system. It is justified to state that ID (ignition delay) can be considered as the CAD difference between the SOC and SOFD.

After fuel enters the combustion chamber and introduced to an ignition delay period during which fuel is heated, evaporated and mixed with air, start of premixed combustion occurs at 3.3 bTDC with an ignition delay period of 6.7 CAD. In this case, the majority of fuel burnt at a premixed combustion mode since fuel had enough time to mix with air during the ignition delay period. Figure (4.10) shows a zoomed view to show the start of injection, start of fuel delivery and start of combustion events

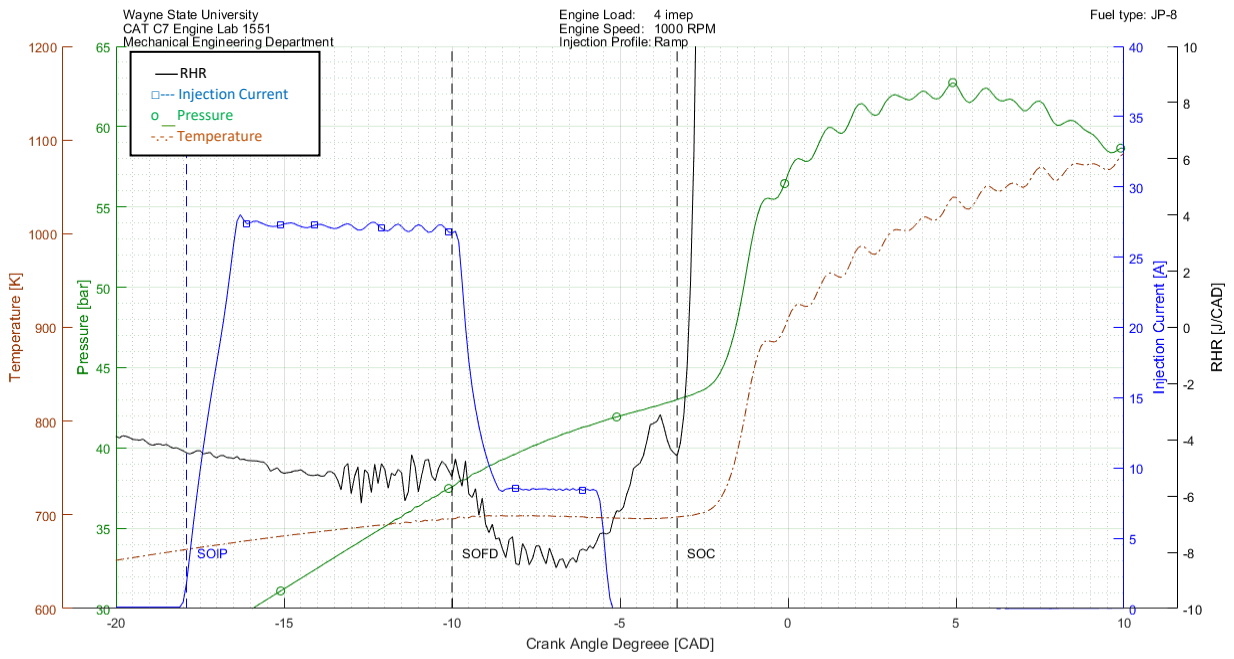

Speed:1000 RPM Load: 4 IMEP Injection Profile: Ramp Fuel: JP-8

Figure 4. 10 Start of injection, start of fuel delivery and start of combustion

4.3.3 **Sample data**

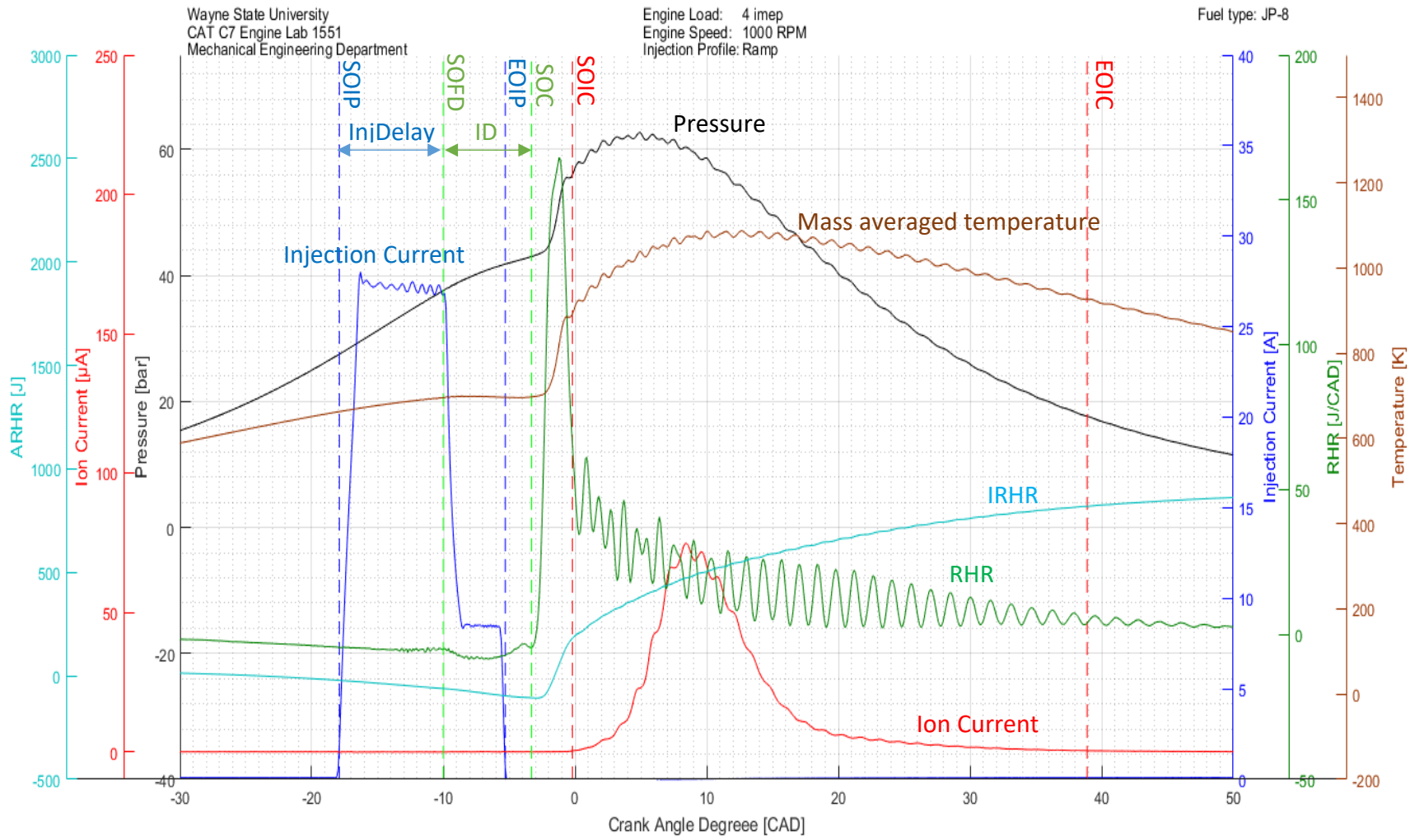

Speed:1000 RPM Load: 4 IMEP Injection Profile: Ramp Fuel: JP-8

Figure 4. 11 Sample data of combustion ionization at 1000 rpm 4IMEP load

Variable	Definition
SOIP	Start of injection pulse
SOFD	Start of fuel delivery
InjD	Injection delay
SOC	Start of combustion
ID	Ignition delay
SOIC	Start of ion current
EOIC	End of ion current

Table (4.1) Definitions

Start of ion current signal (SOIC) is determined using the expression

SOIC = [Threshold (@SOI) +0.2 µA] * 120% (19) [2]

Badawy et al [2] developed and used equation (19) to determine the start of ion signal and used this value to control the injection command of a common rail diesel engine at steady state and transient load conditions

4.3.4 Effect of load at low load conditions

The following figures show the experimental data recording in-cylinder pressure, ion current signal, and injection pulse. Also shown the calculated apparent rate of heat released, calculated mass average temperature and integrated rate of heat released from IVC to EVO to study the characteristics of ion current signal at a single injection utilizing a ramp injection rate profile. Averages of 100 cycle were calculated with the engine running at steady state at a constant speed and four different load points.

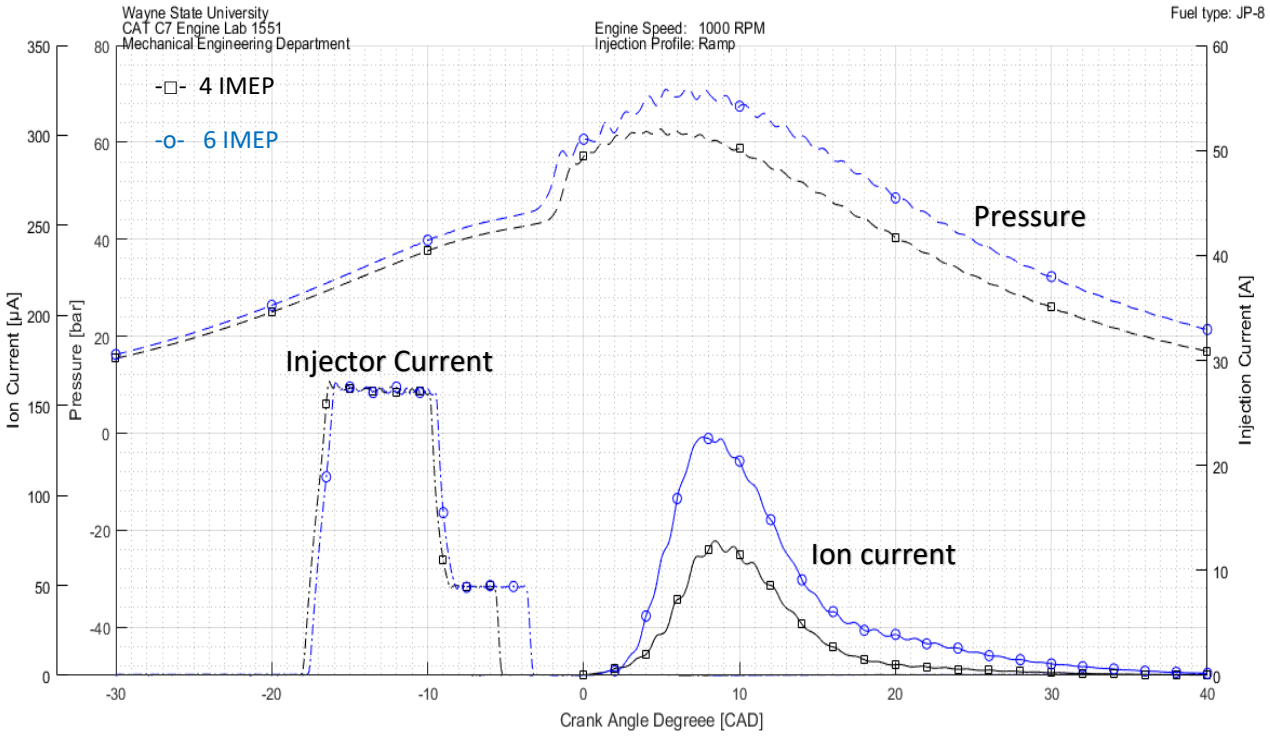

Figure 4. 12 Effect of load on combustion pressure and ion current

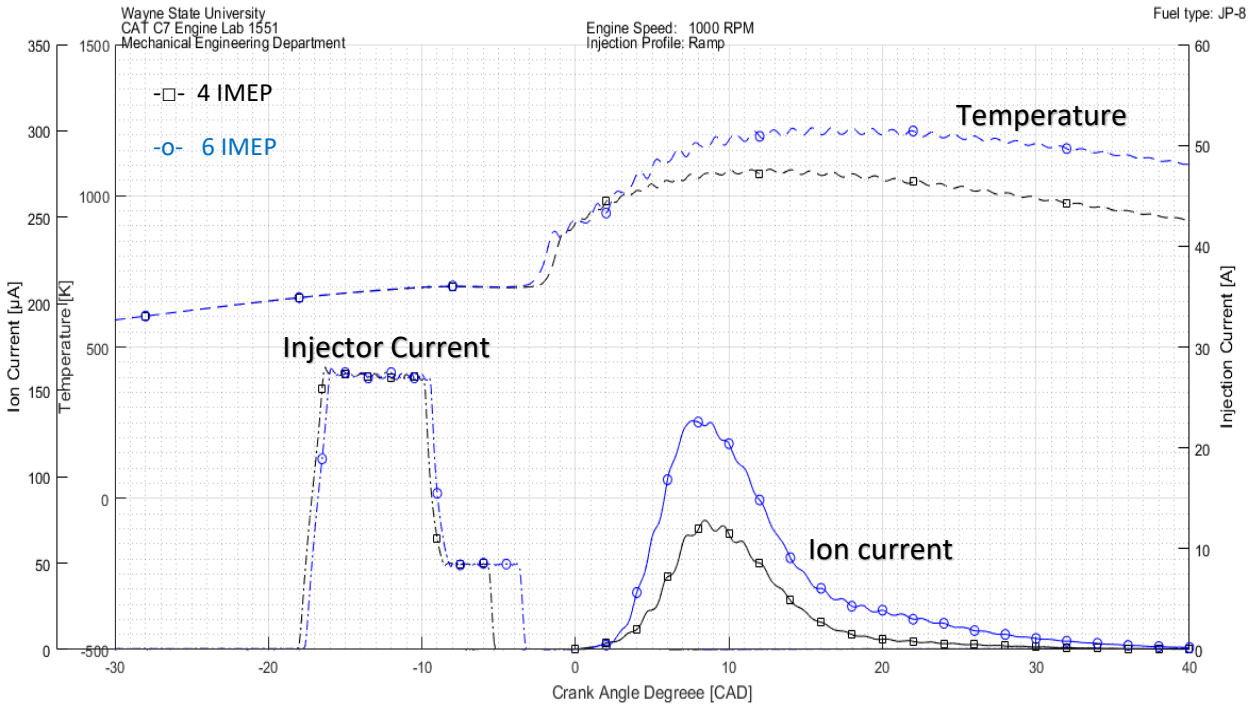

Speed:1000 RPM Load: 4-6 IMEP Injection Profile: Ramp Fuel: JP-8

Figure 4. 13 Effect of load on temperature and ion current

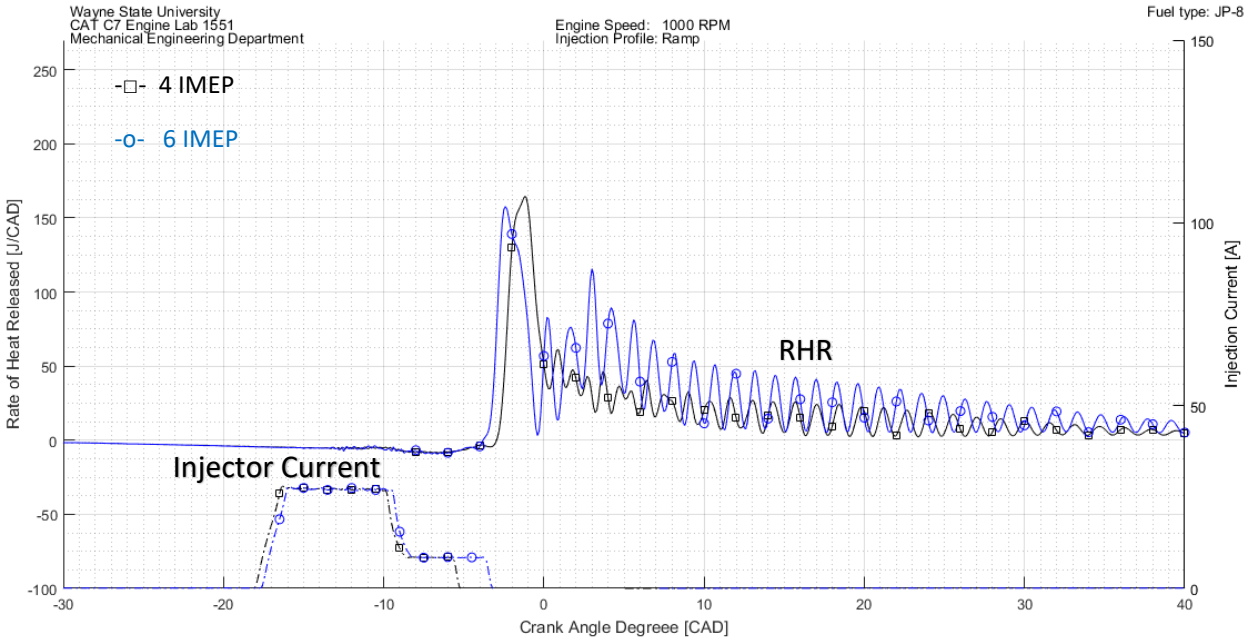

Speed:1000 RPM Load: 4-6 IMEP Injection Profile: Ramp Fuel: JP-8

Figure 4. 14 Effect of load on RHR and ion current

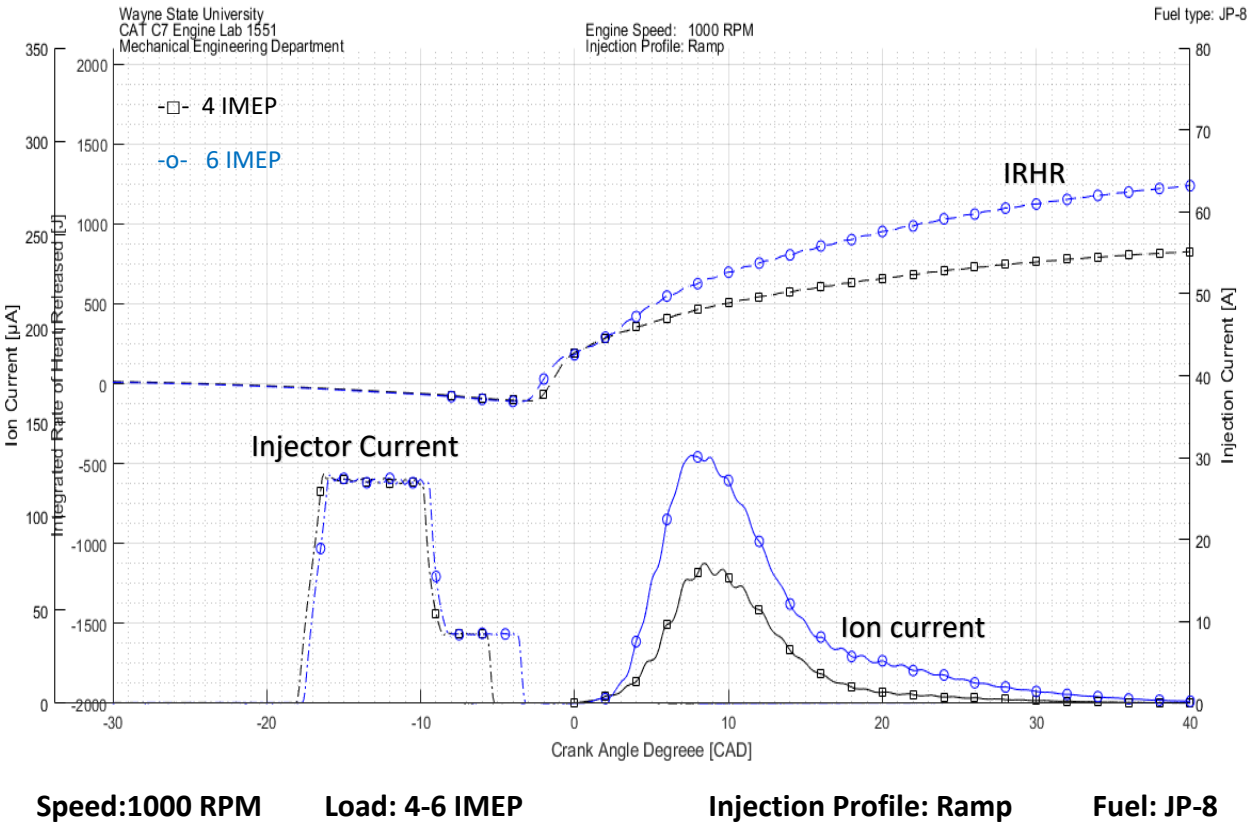

Figure 4. 15 Effect of load on IRHR and ion current

At low engine load conditions, premixed combustion is the dominant combustion regime since small amounts of fuel are injected with enough time for evaporation and mixing with air. It is clearly shown a single peak for the rate of heat released traces in figure (4.14) of 164.67 J/CAD for 4 IMEP load and reduced to 157.68 J/CAD for 6 IMEP.

In this case increasing the load by injecting more fuel had its effects on increasing the in-cylinder pressure shown in figure (4.12) and calculated in-cylinder mass averaged temperature. Both the pressure and temperature traces show a sharp rise close to TDC as a result of the premixed combustion of the fuel which occurred at 3.3 bTDC and 4 bTDC for 4 and 6 IMEP respectively.

With more fuel injected into the combustion chamber to obtain higher load, only a fraction of the fuel would have enough time during the ignition delay period to evaporate and mix with air leading to a premixed combustion as discussed earlier. However, the rest of the fuel would burn due to the high temperature diffusion introducing a second mode of combustion which is the diffusion combustion mode.

It is also noted that the reduction in the premixed combustion peak is accompanied by an increase in the diffusion combustion peak to reach 115.63 J/CAD however, the premixed combustion is still the dominant regime.

Since ion signal peak is sensitive to temperature [2], the change in ion signal peak was recorded to be 74.79 μA for the 4 IMEP load point and 132.37 μA for 6 IMEP load point. The ion signal showed only one peak since the premixed combustion is the dominant regime at low loads and it is hard to distinct between the premixed and diffusion combustion modes at such low load conditions.

4.3.5 Effect of load at medium load conditions

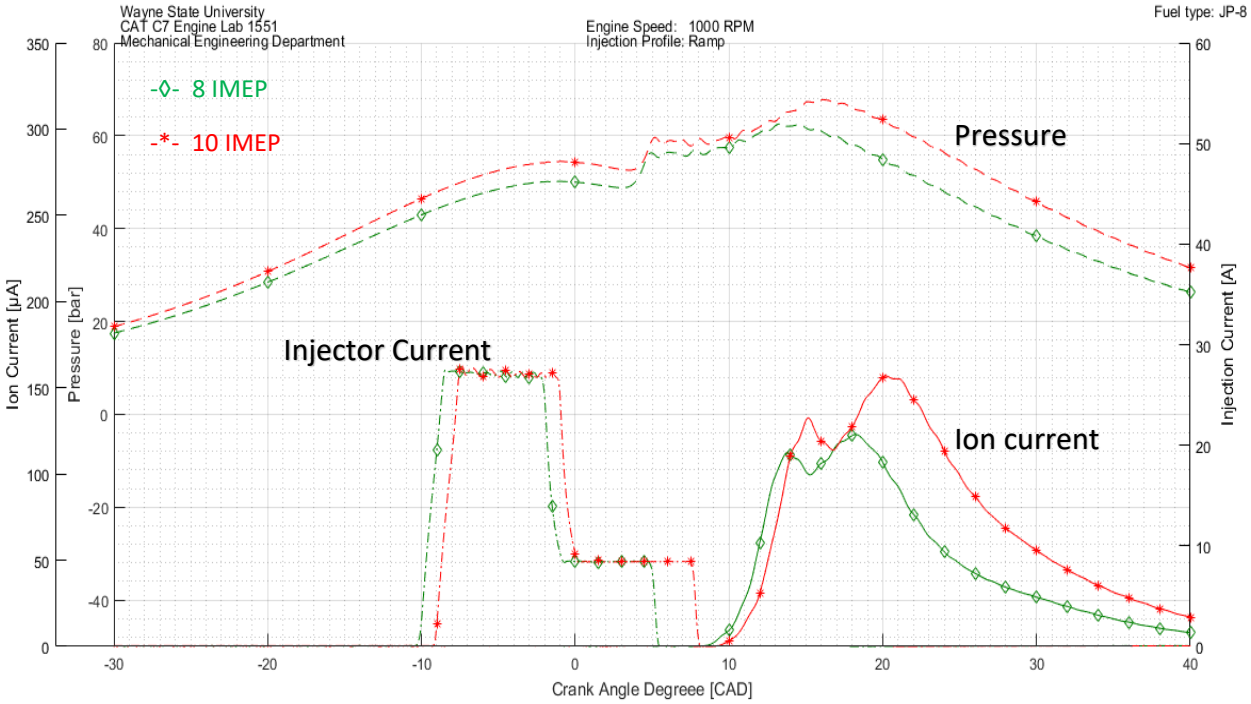

Figure 4. 16 Effect of load on combustion pressure and ion current

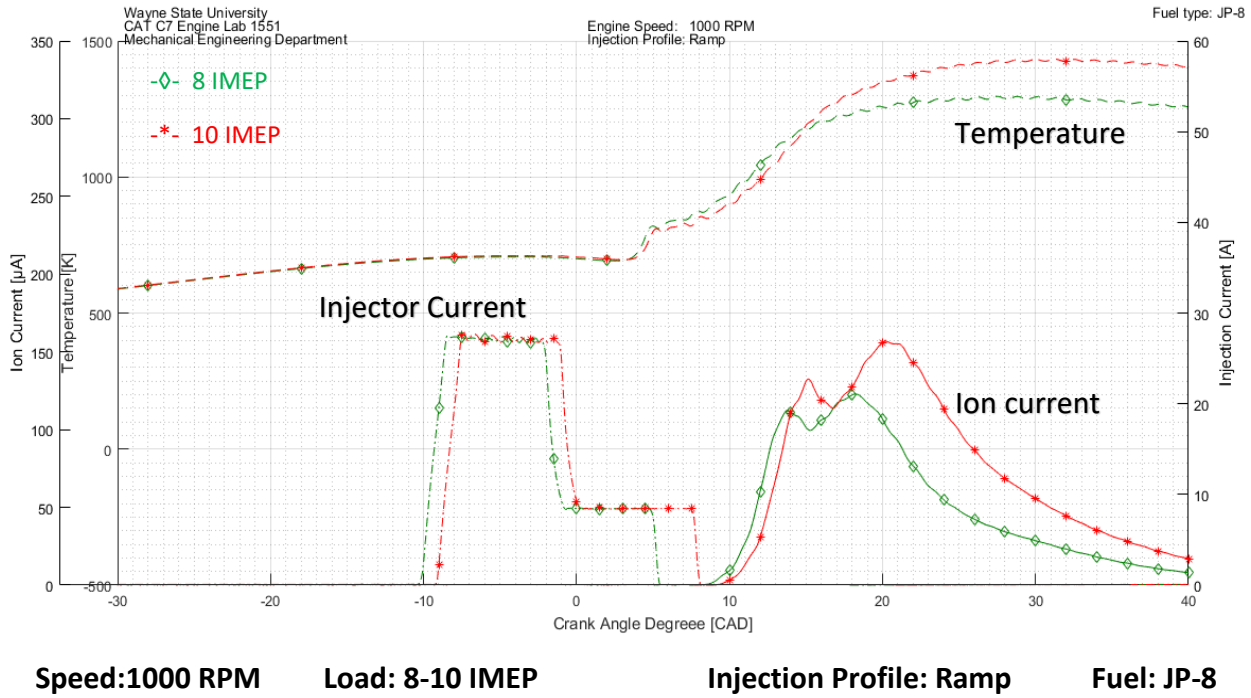

Figure 4. 17 Effect of load on temperature and ion current

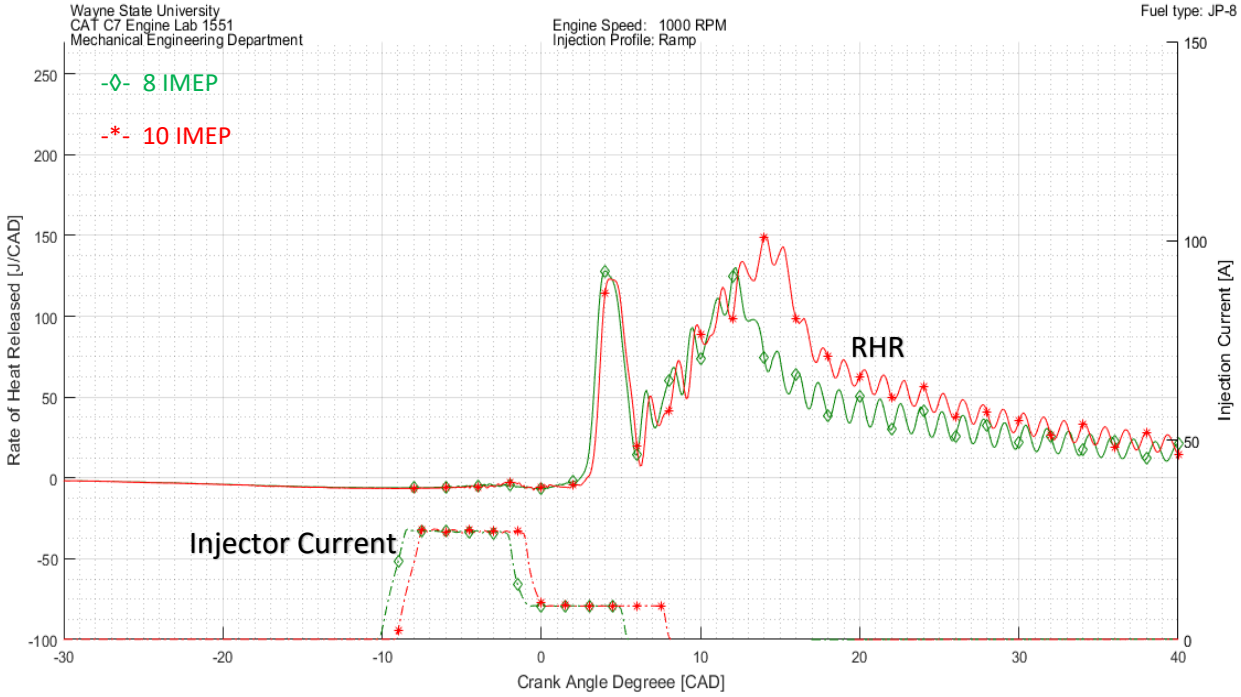

Figure 4. 18 Effect of load on RHR

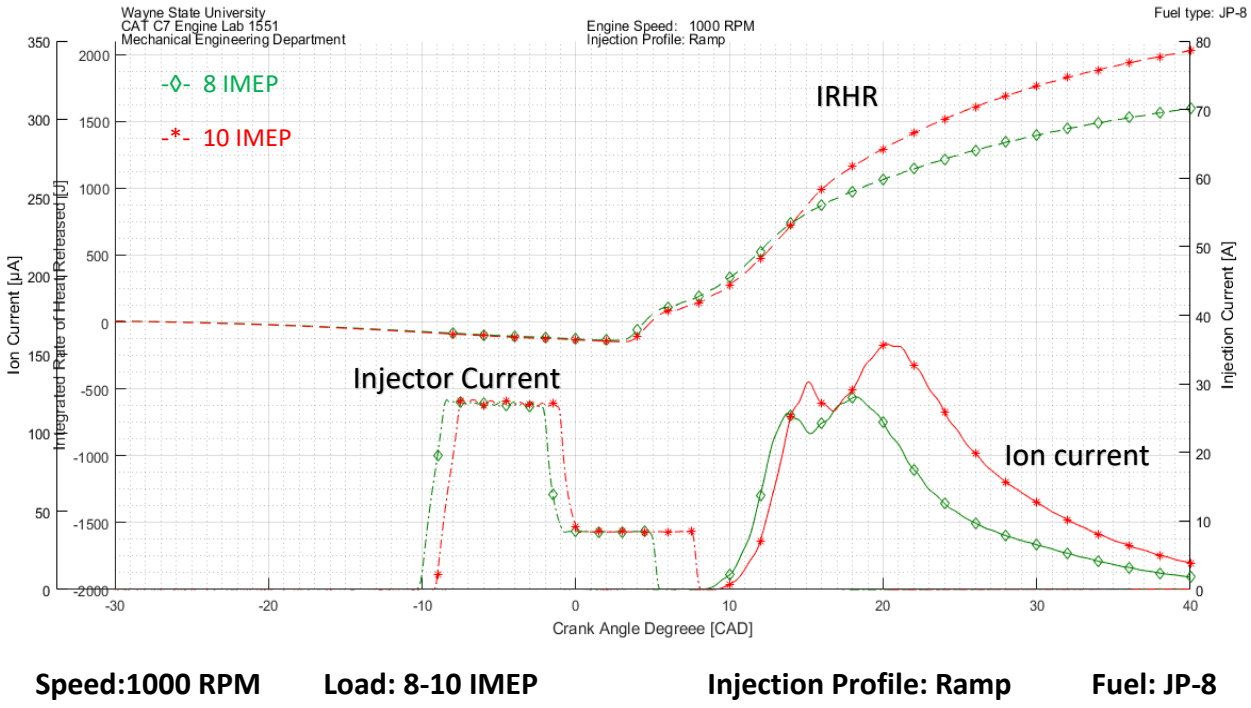

Figure 4. 19 Effect of load on IRHR and ion current

At medium and high engine load conditions, it is fairly easy to differentiate between premixed and diffusion combustion modes from the signal traces. Pressure and temperature traces in figures (4.16) and (4.17) show a sharp increase due to the premixed combustion mode followed by the slower rise and reached the peak due to the diffusion combustion mode. Shown in figure (4.18) two peaks in the rate of heat released traces representing the different combustion regimes

Ion current signal showed an increase in amplitude values along with the temperature and pressure as an effect of increasing engine load. Also noted that ion current signal shows two distinct peaks representing the two modes of combustion.

Rate of heat released peak of premixed combustion showed a reduction in peak value accompanied with an increase in the diffusion combustion peak.

4.3.6 Results and observations

Noted from the previous figures that injection duration is increased to obtain high engine load allowing more fuel to be injected into the combustion chamber as the amount of fuel injected depends on the injection pressure and injection duration.

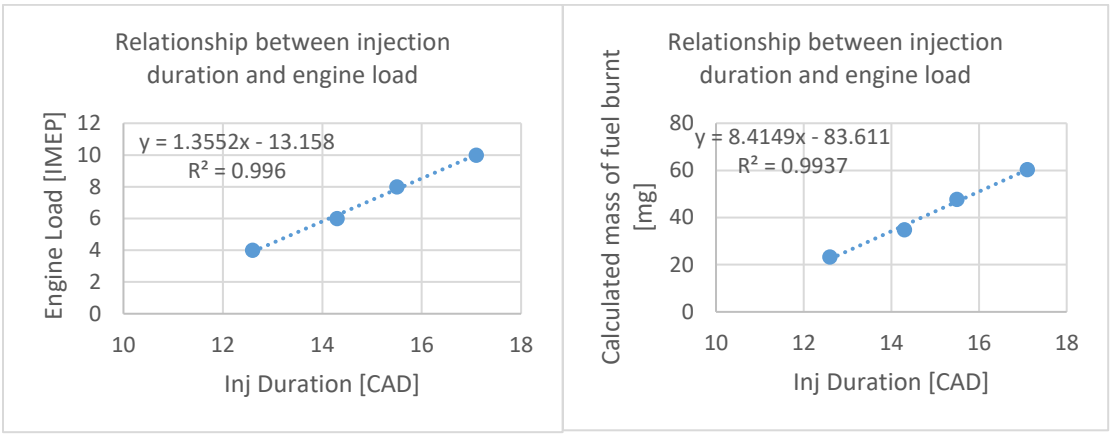

Figure 4. 20 Effect of injection duration on engine load and amount of fuel burnt

In this study SOIP couldn`t be held constant since the production ECU of the Caterpillar C7 engine was used to run the engine.

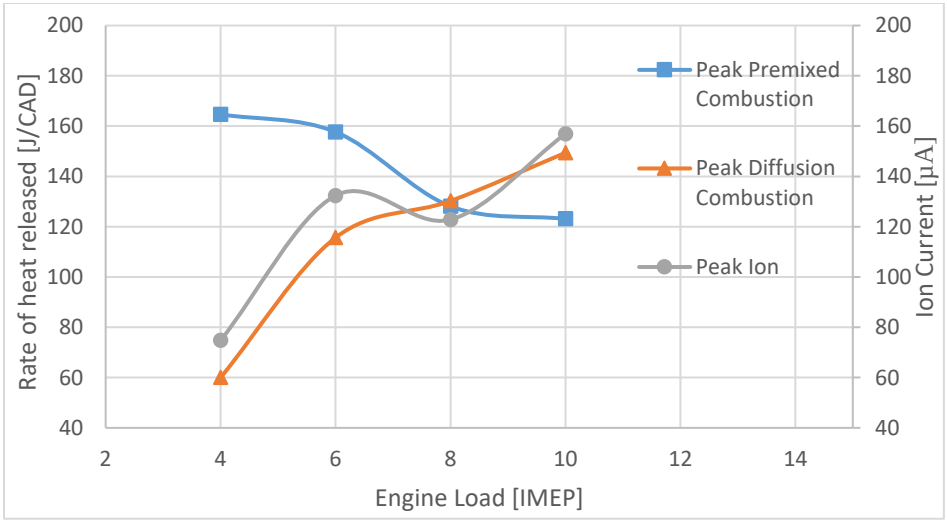

Figure 4. 21 Relation between RHR peaks and Ion current signal peak

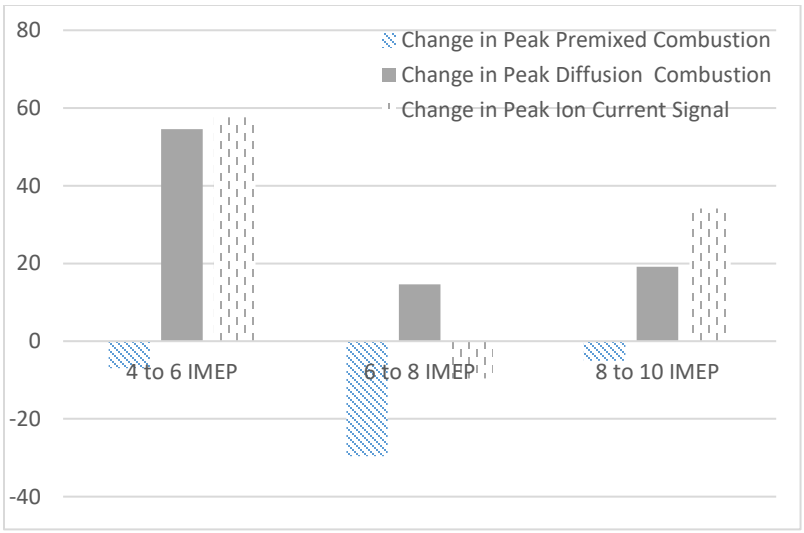

Figure 4. 22 Relation between RHR peaks and Ion current signal peak

As discussed earlier, as an effect of increasing engine load, peak premixed combustion decreases while peak of diffusion combustion increases. Figures (4.21) and (4.22) explain the results of comparing the change in peak of premixed combustion and diffusion combustion peaks showing a reasonable study of the effect of load on the characteristics of the ion current signal. While engine load was increased from 4 to 6 IMEP a 54.53 J/CAD increase in diffusion combustion peak had the dominant effect on the increase of ion current signal peak of 57.58 µA compared to the decrease in premixed combustion peak of 6.99 J/CAD. In another scenario where engine load was increased from 6 to 8 IMEP, the same concept applies but in the other way around. The effect of decreasing change of premixed combustion peak is the dominant allowing the ion signal peak to decrease. Then back again to the increase of ion signal peak as the load was increased from 8 to 10 IMEP where diffusion combustion increasing change was dominant.

Also concluded from the results strong correlations between SOIC-SOC and SOIC-SOFD enhancing the capabilities of the ion current sensor to perform combustion phasing and act as a combustion timing sensor for multi fuel operation.

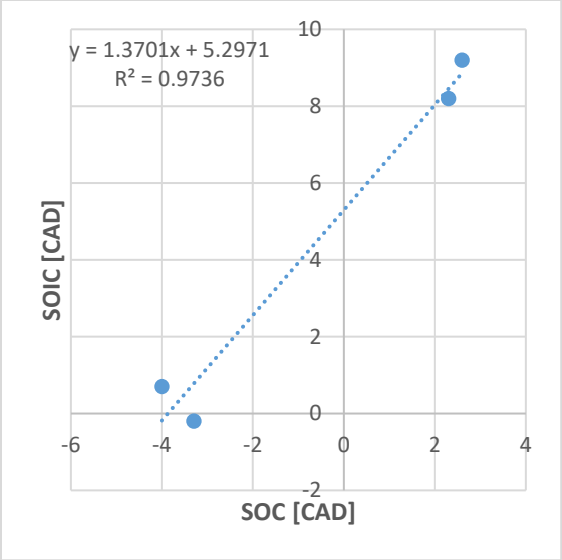

Figure 4. 23 SOC-SOIC correlation

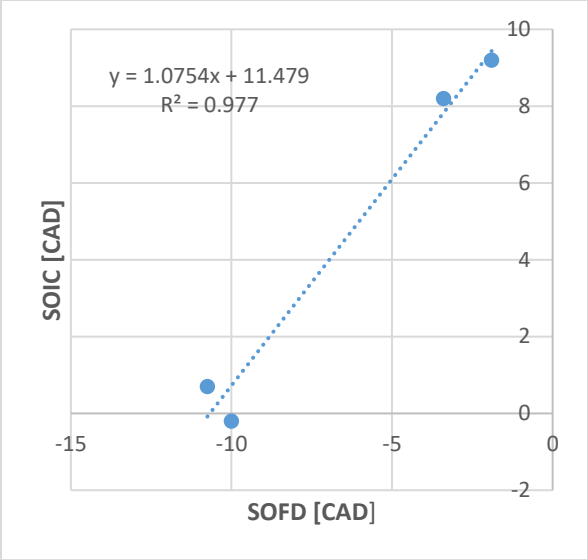

Figure 4. 24 SOFD-SOIC correlation

Shown in figures (4.23), (4.24) linear trend lines fitted to the SOC-SOIC and SOFD-SOIC correlations having coefficient of determination, R^2 of 97.36% and 97.7% respectively. These correlations were studied for low and medium load conditions only.

4.4 Single square profile injection

4.4.1 HEUI Injector operation

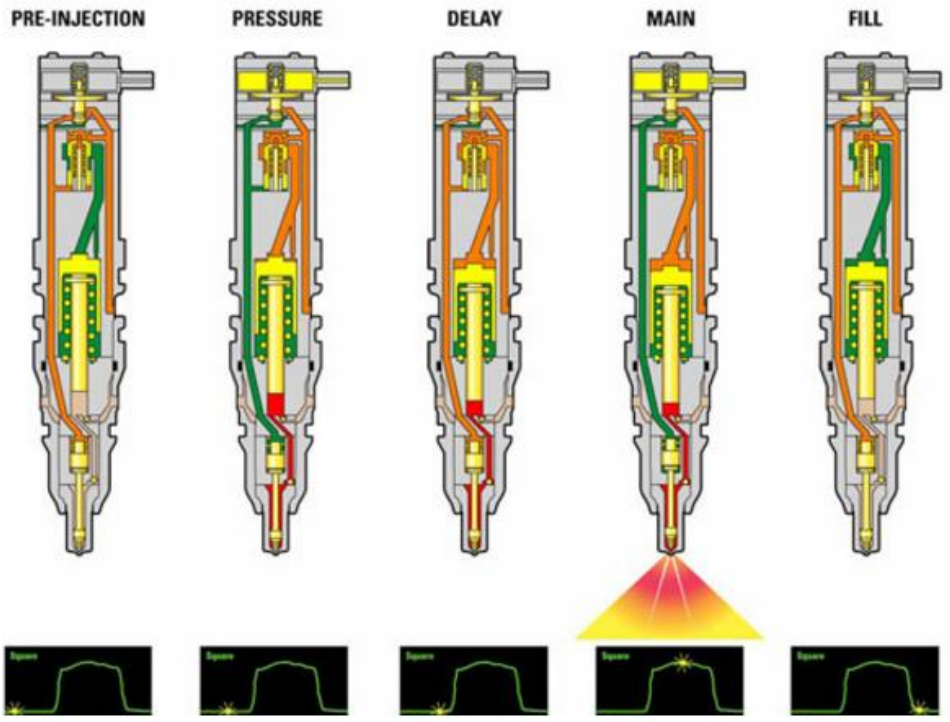

Figure 4. 25 Single square injection event [13]

In order to obtain a single injection with the square profile, two current waveforms are provided to the solenoid as shown in figure (4.26)

Pre-Injection: As mentioned earlier in the pre-injection stage of the ramp profile with the control valve blocking the intensifier chamber and also high pressure oil is closing the needle.

Pressure: Actuation oil travels through the oil supply line through the injector body passing through the spool control valve acting on the intensifier plunger thus pressurizing the fuel when a short current command energizes the solenoid. Although the spool valve opened the way to the oil to push the intensifier plunger downwards, the pressurization

rate is low and not sufficient to overcome the forces acting on the check piston and hence, fuel is not delivered to the combustion chamber.

Delay: At this stage, the solenoid is de-energized for some delay time causing the seated pin to move upwards, and this, in turn, allows the oil to pressurize the check line keeping the needle closed in spite of pressure build up on the fuel.

Main: A second current waveform is supplied to the injector solenoid after the short delay. Again, energizing the solenoid pulls the seated pin to the upper seat allowing the main injection to occur followed by the fill stage as explained earlier.

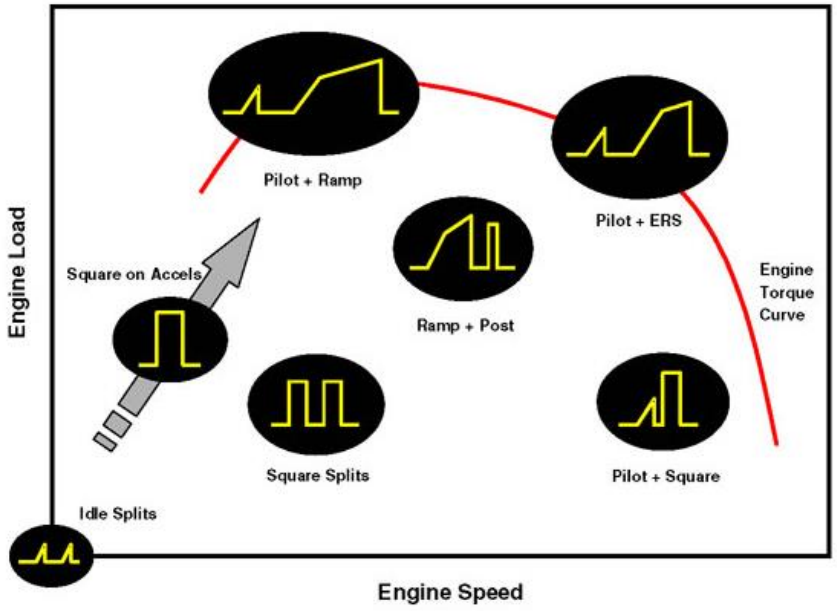

Figure 4. 26 Injection rate and events map of Caterpillar HEUI-B [13]

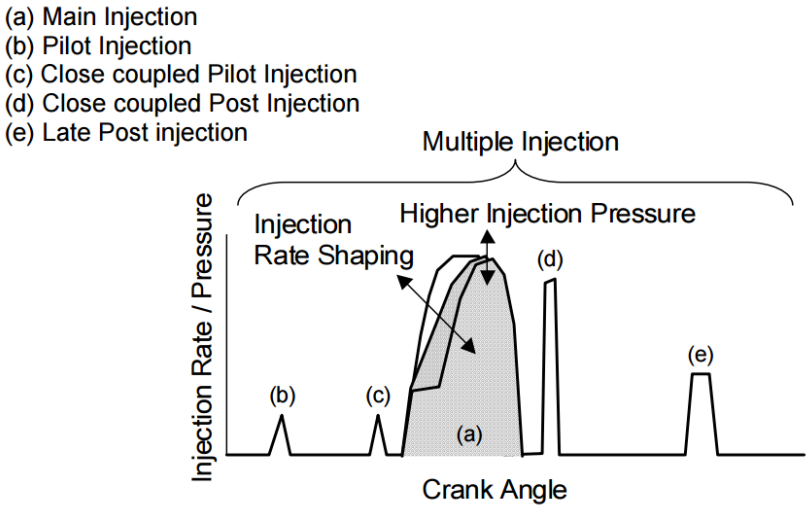

Figure 4. 27 Multiple injection events and main injection rate shaping [14]

Tanabe et al. [14] demonstrated the effects of changing the rate shape of the main fuel injection event on the engine-out emissions as ramp and boot profiles can decrease the NOx emissions because smaller amount of fuel is injected during the ignition delay period resulting in a lower premixed combustion in the rate of heat released curve. The authors also found out that ramp profile is preferred at low engine speed low load conditions, boot profile is preferred at low speed high load conditions and square profile is preferred at high speed high load conditions.

To study the characteristics of the square injection profile, the resistor connected across the engine coolant temperature sensor was removed to allow the ECU to operate at normal warm conditions.

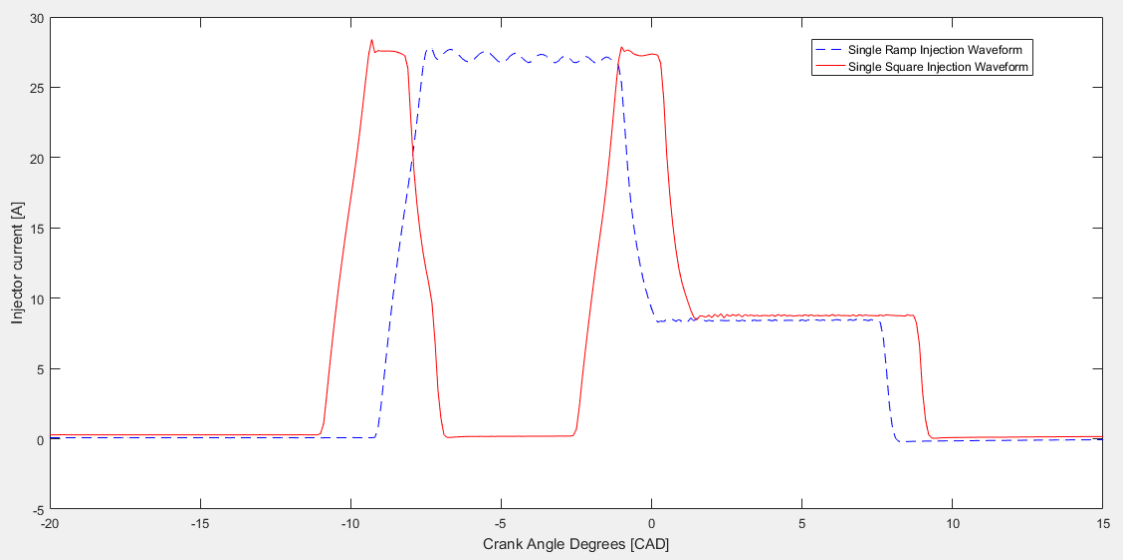

Figure 4. 28 Ramp and Square injection waveform

As discussed earlier, two current waveforms supplied to the injector solenoid to perform a square injection profile shown in figure (4.28). Also, it is found that the solenoid opening current duration for square and ramp injection profiles are different.

With the ECU performing at normal operating conditions and measuring higher coolant temperature, the higher coolant temperature the higher injection actuation oil temperature, which concludes that oil would have lower viscosity making the actuation process faster and doesn`t need such electrical power provided to the solenoid to open the spool control valve.

Stockner et al [17] studied the system sensitivity to oil viscosity for cold temperature operation and provided a strategy to take into consideration the injector response at different actuation oil viscosity and temperatures by adjusting injection timing.

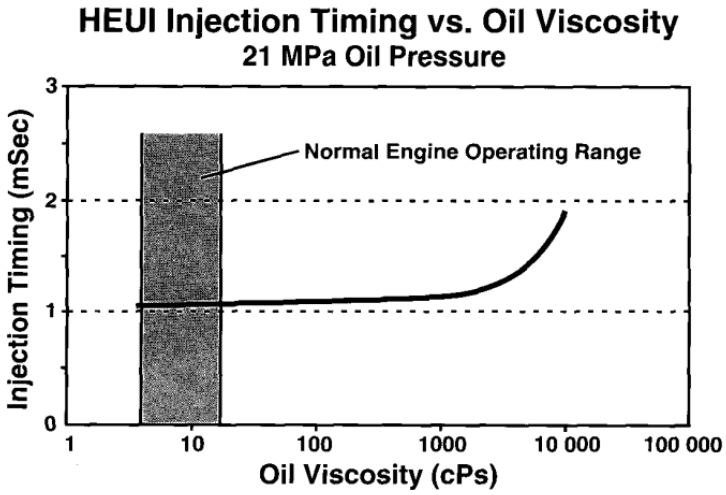

Figure 4. 29 Effect of oil viscosity on HEUI injection timing [17]

4.4.2 Effect of load at low load conditions

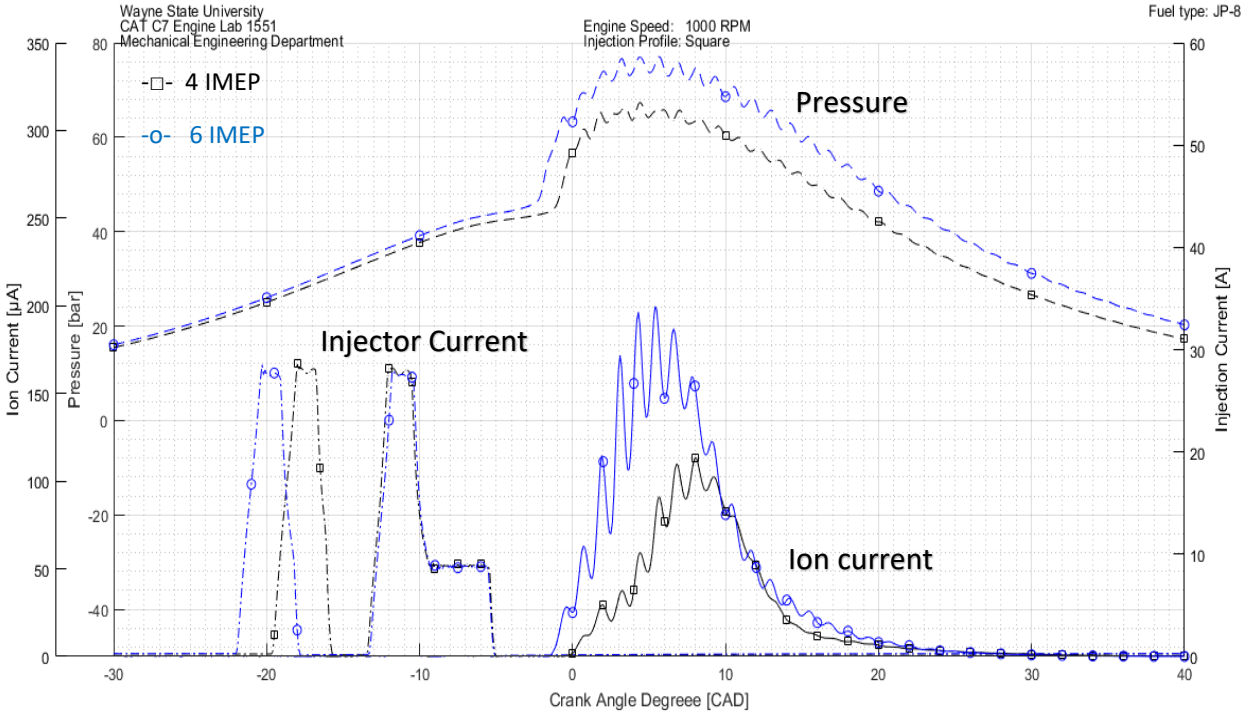

Figure 4. 30 Effect of load on combustion pressure and ion current

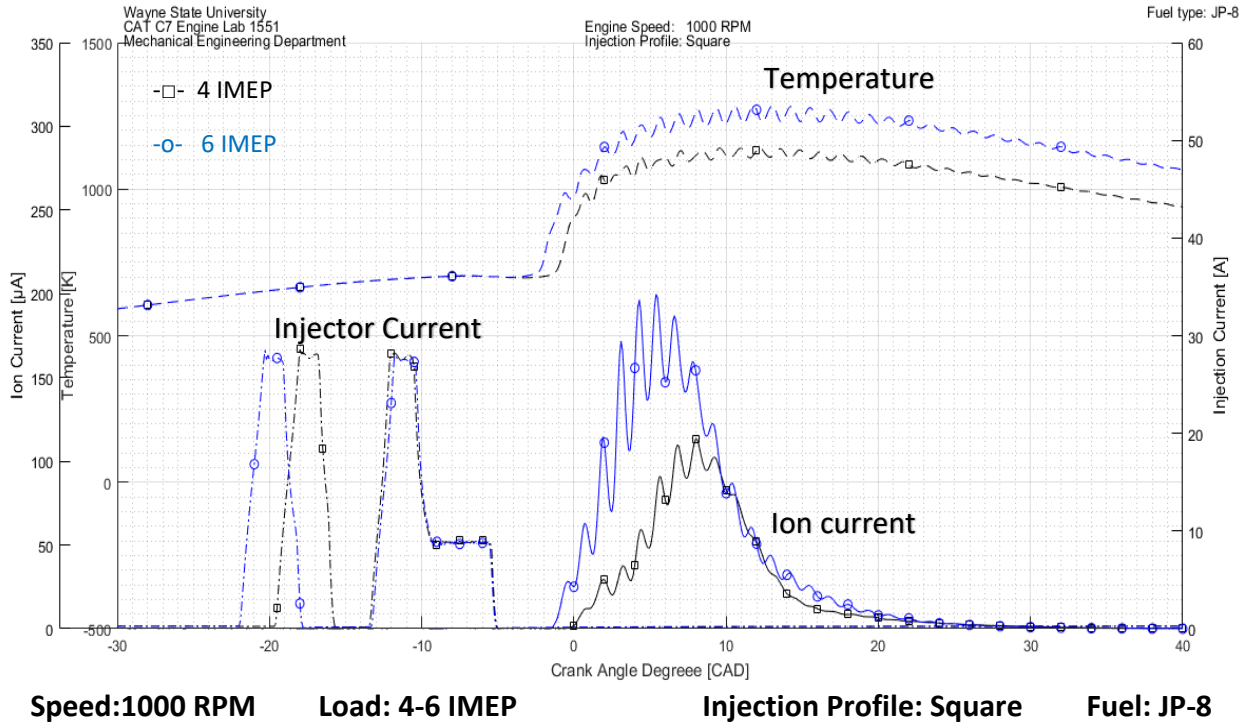

Figure 4. 31 Effect of load on temperature and ion current

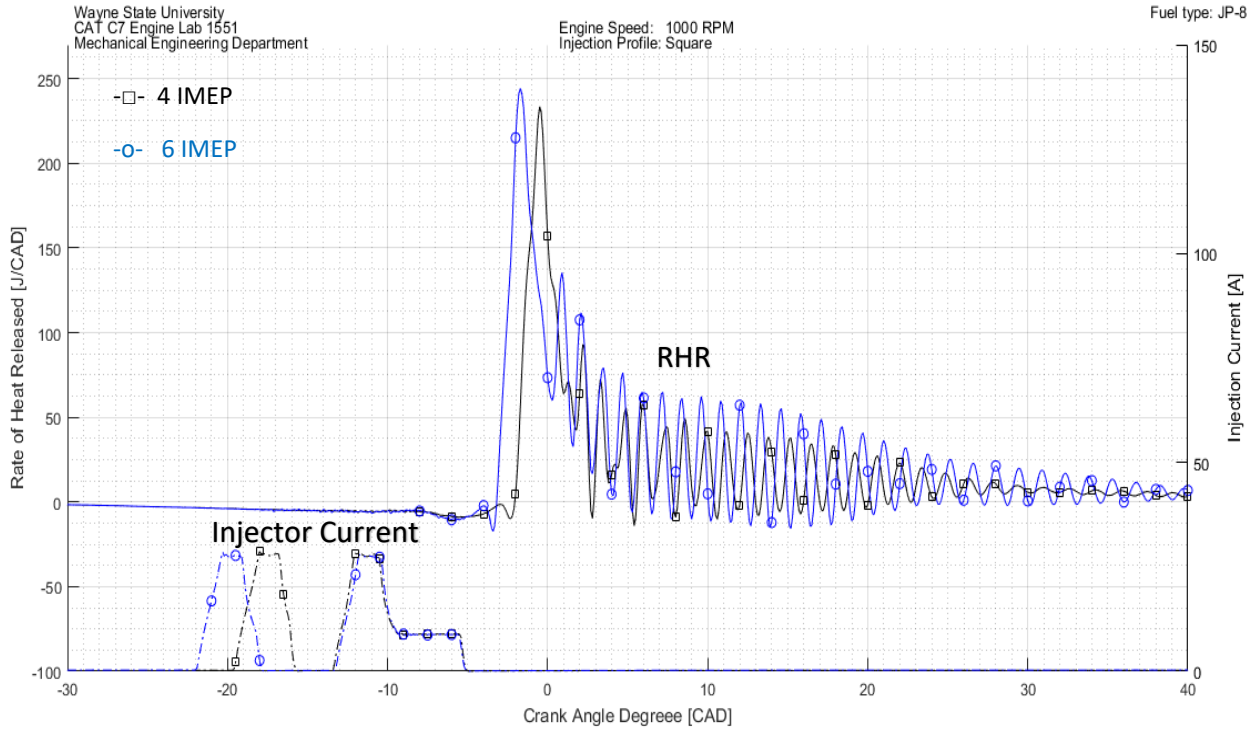

Figure 4. 32 Effect of load on RHR and ion current

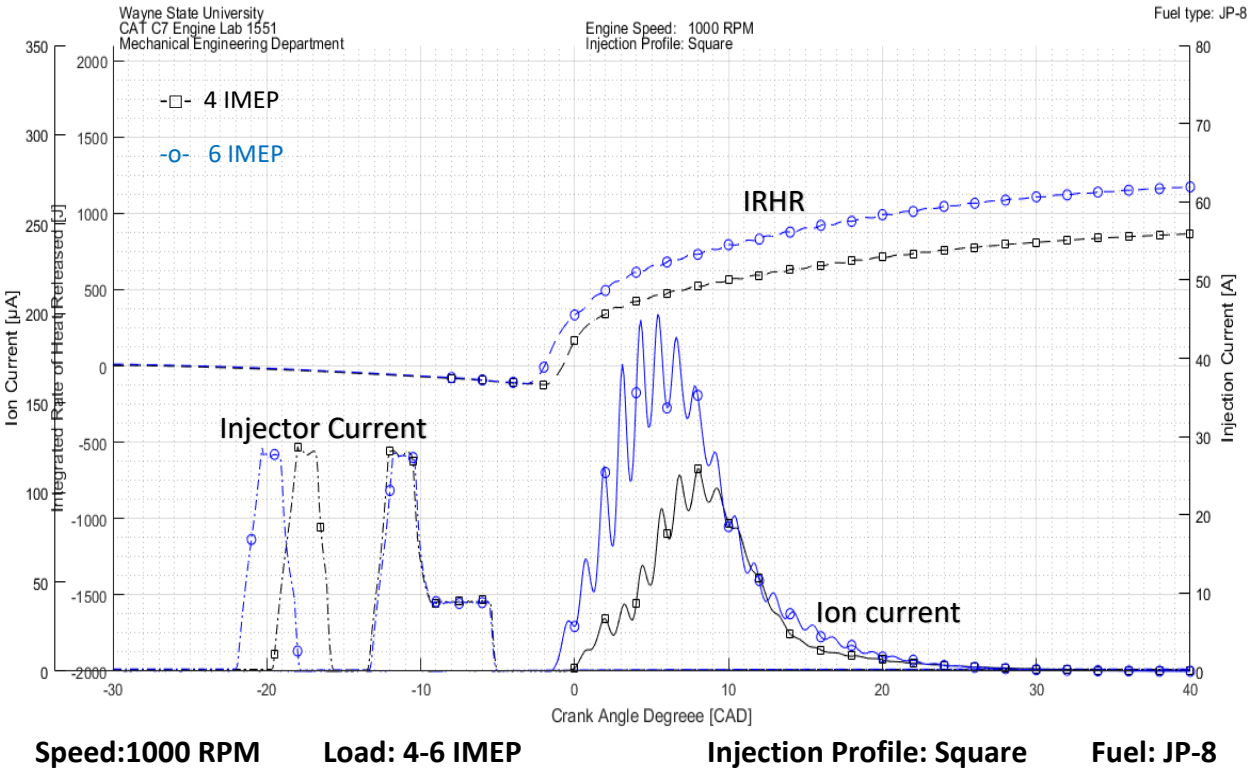

Figure 4. 33 Effect of load on IRHR and ion current

The effect of load on the characteristics of ion current signal was studied at steady state same speed and load conditions utilizing fast injection rate profile “Square profile”. Figure (4.30) shows the effect of increasing the load on combustion pressure with respect to the ion current signal. Figure (4.31) shows the increase in combustion temperature as more fuel is injected and burnt. Also, figure (4.32) the calculated rate of heat traces with showing single peak due to the premixed combustion of the fuel and no distinct peaks for the diffusion combustion. Figure (4.33) shows the integrated rate of heat released which indicates the amount of fuel burnt due to the combustion to be compared with the amount of fuel burnt in the ramp injection profile.

4.4.3 Effect of load at medium load conditions

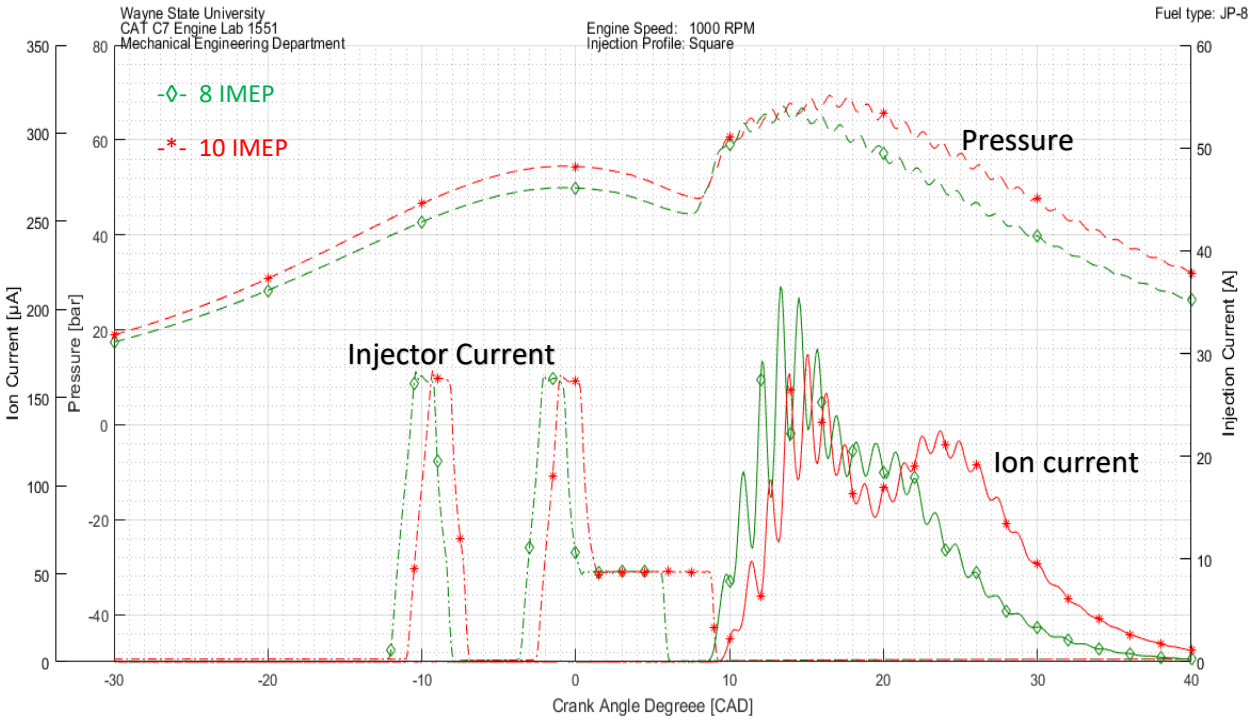

Speed:1000 RPM Load: 8-10 IMEP Injection Profile: Square Fuel: JP-8

Figure 4. 34 Effect of load on combustion pressure and ion current

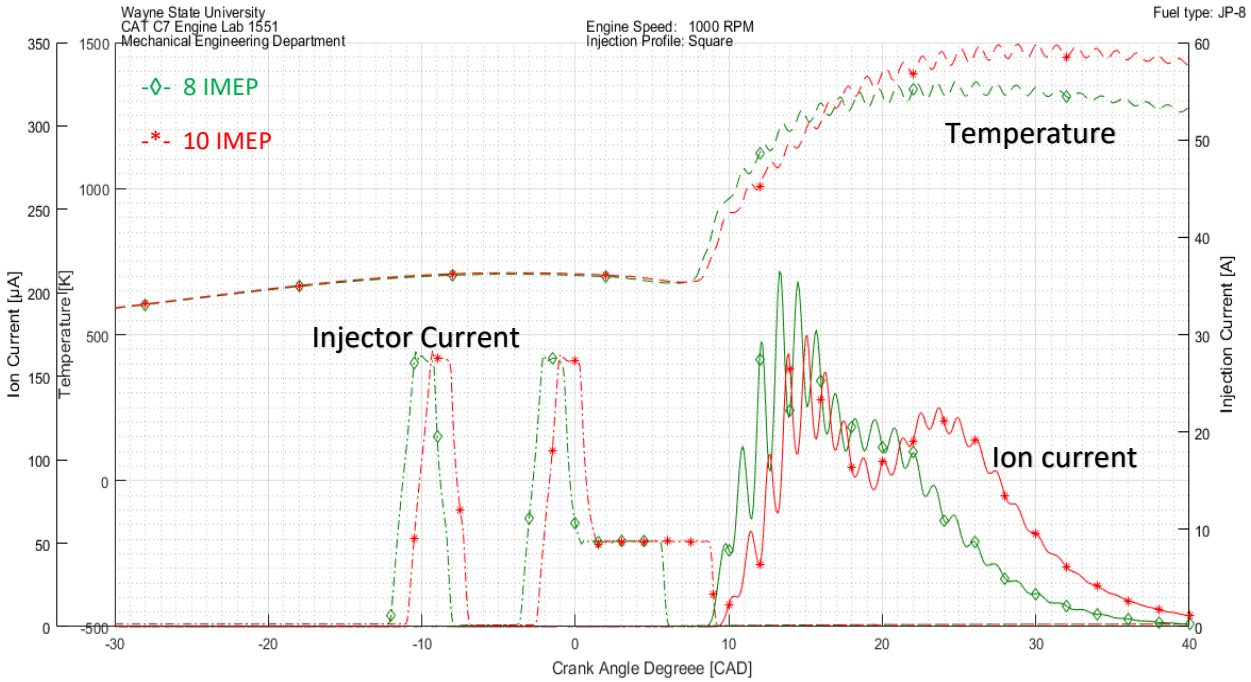

Figure 4. 35 Effect of load on temperature and ion current

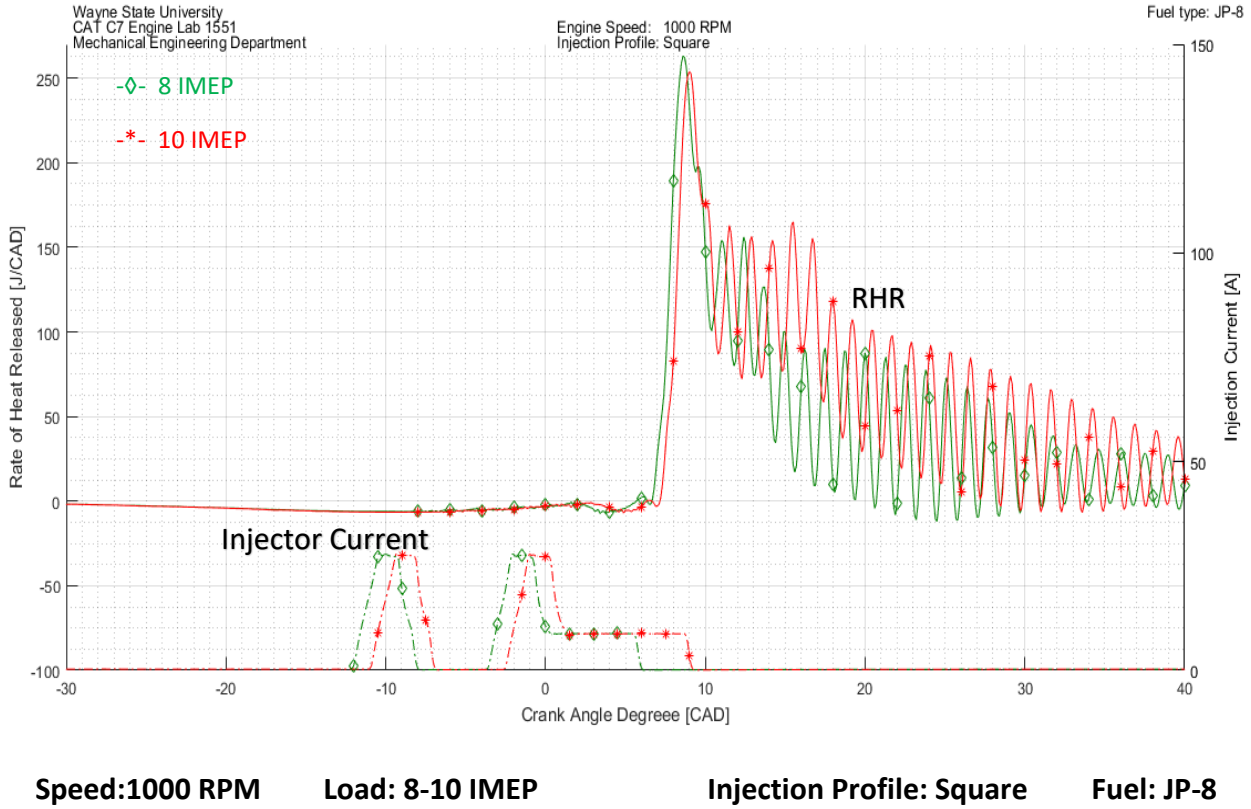

Figure 4. 36 Effect of load on RHR

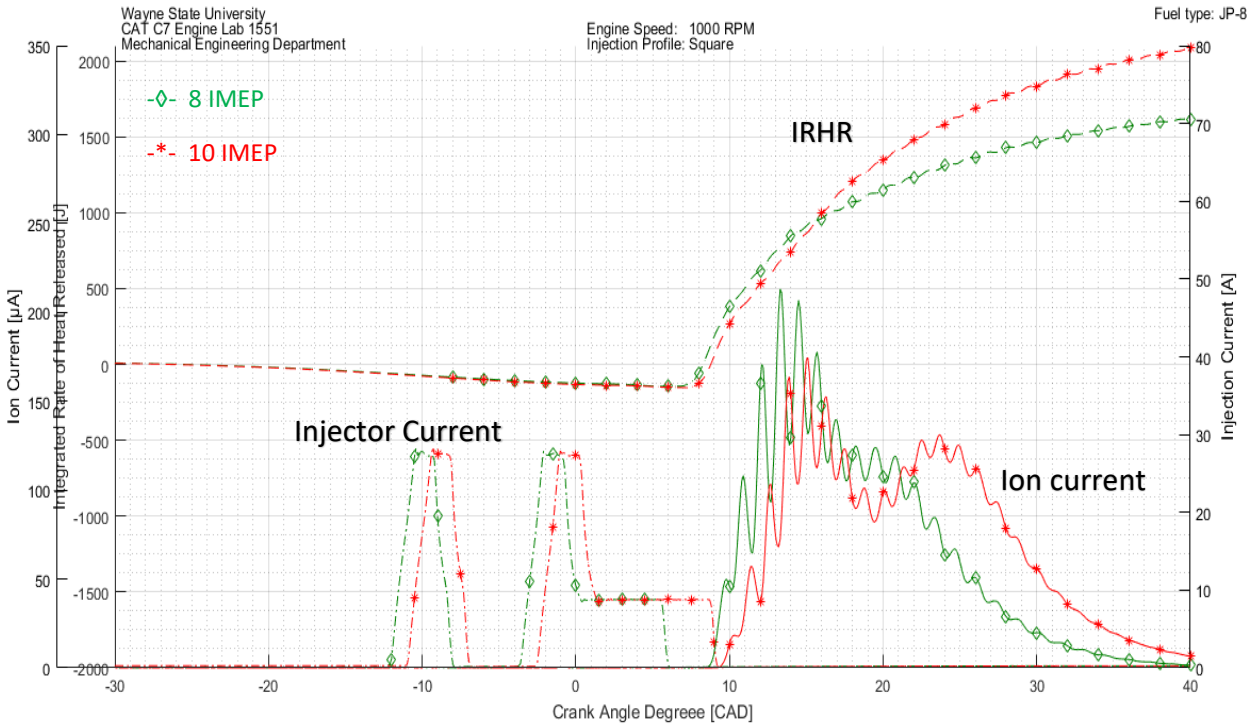

Speed:1000 RPM Load: 8-10 IMEP Injection Profile: Square Fuel: JP-8

Figure 4. 37 Effect of load on IRHR and ion current

Following the same trend, increasing the load by increasing the amount of fuel injected results in the increase in the peak of premixed combustion at low load conditions and an increase in the ion signal peak.

At medium load conditions, increasing the load leads to the decrease in peak of premixed combustion accompanied by the increase in peak of diffusion combustion. Ion current signal successfully recorded two distinct peaks representing the two modes of combustion.

4.4.4 Effect of injection profile

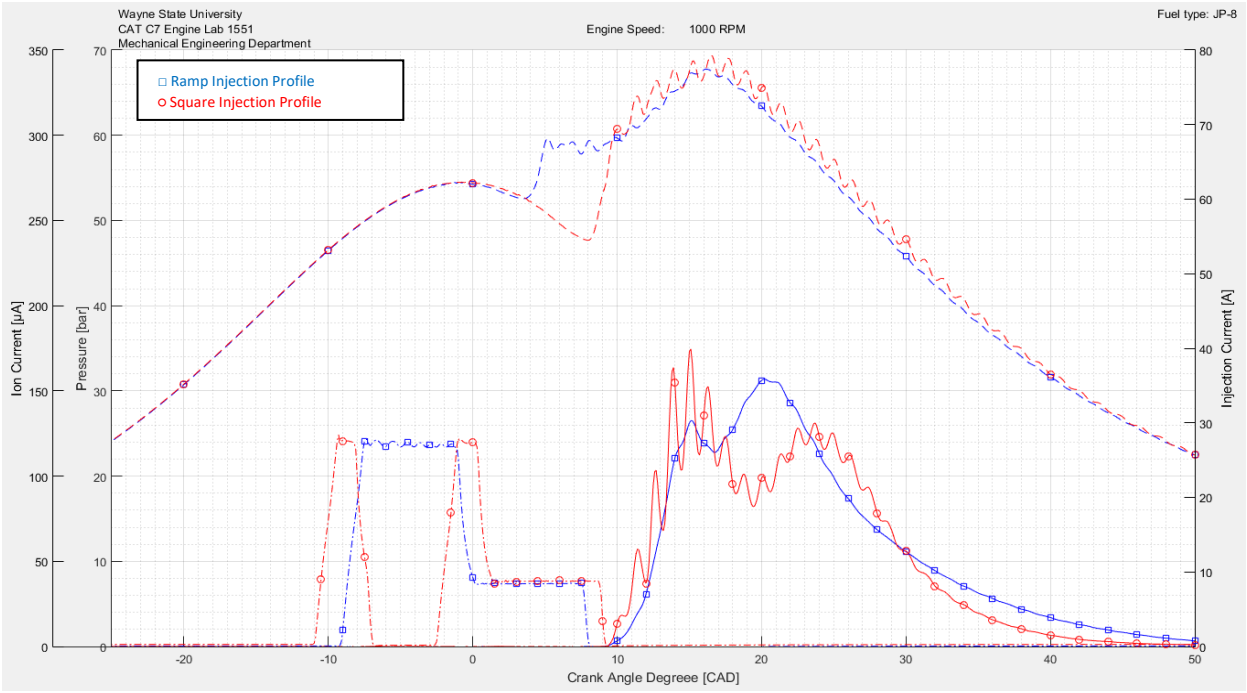

Speed:1000 RPM Load: 10 IMEP Injection Profile: Square Fuel: JP-8

Figure 4. 38 Effect of injection profile on the ion current signal and combustion pressure

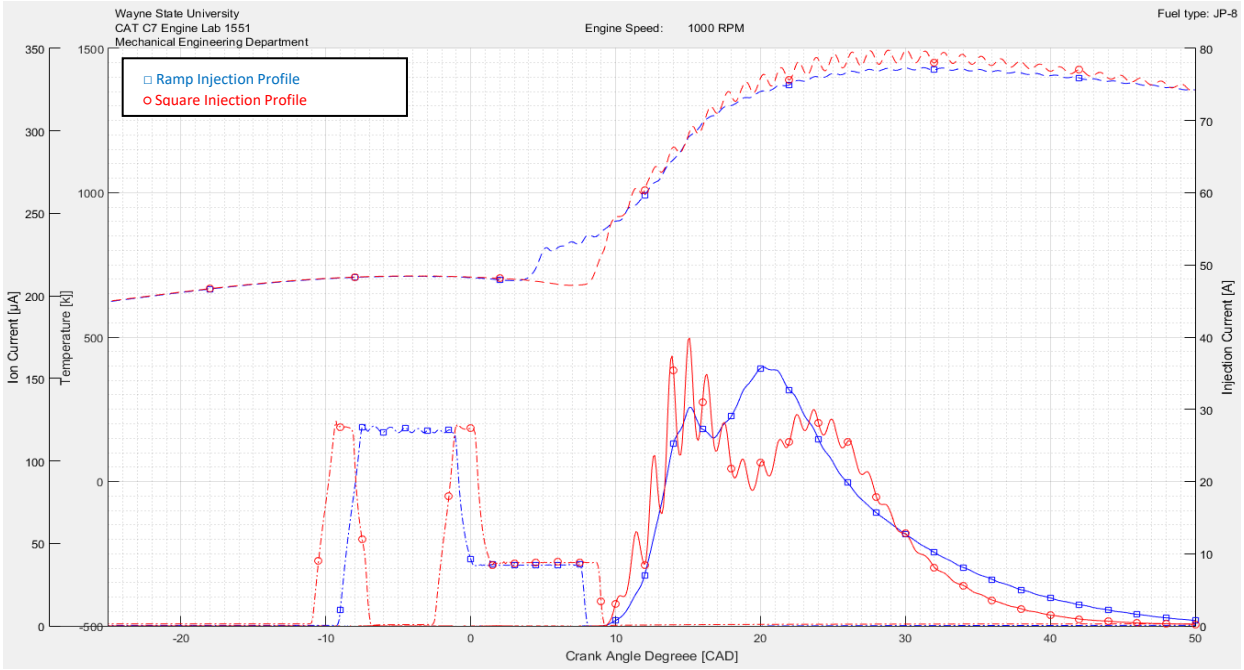

Speed:1000 RPM Load: 10 IMEP Injection Profile: Square Fuel: JP-8

Figure 4. 39 Effect of injection profile on the ion current signal and temperature

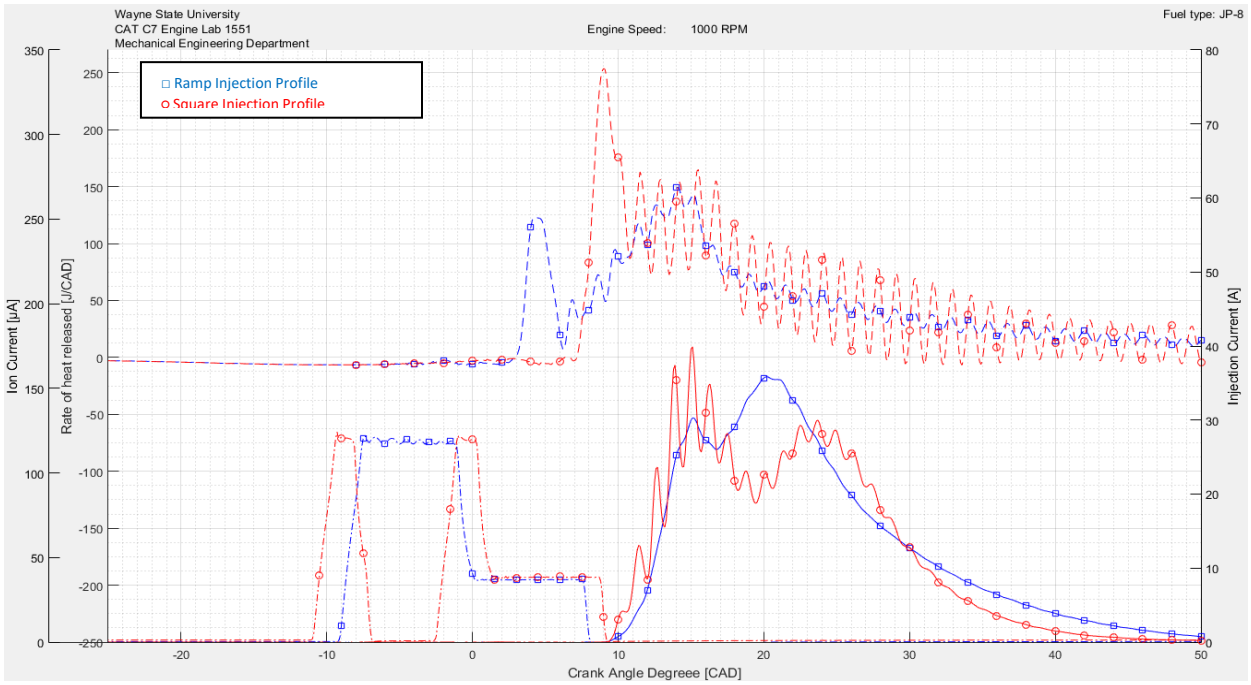

Speed:1000 RPM Load: 10 IMEP Injection Profile: Square Fuel: JP-8

Figure 4. 40 Effect of injection profile on the ion current signal and RHR

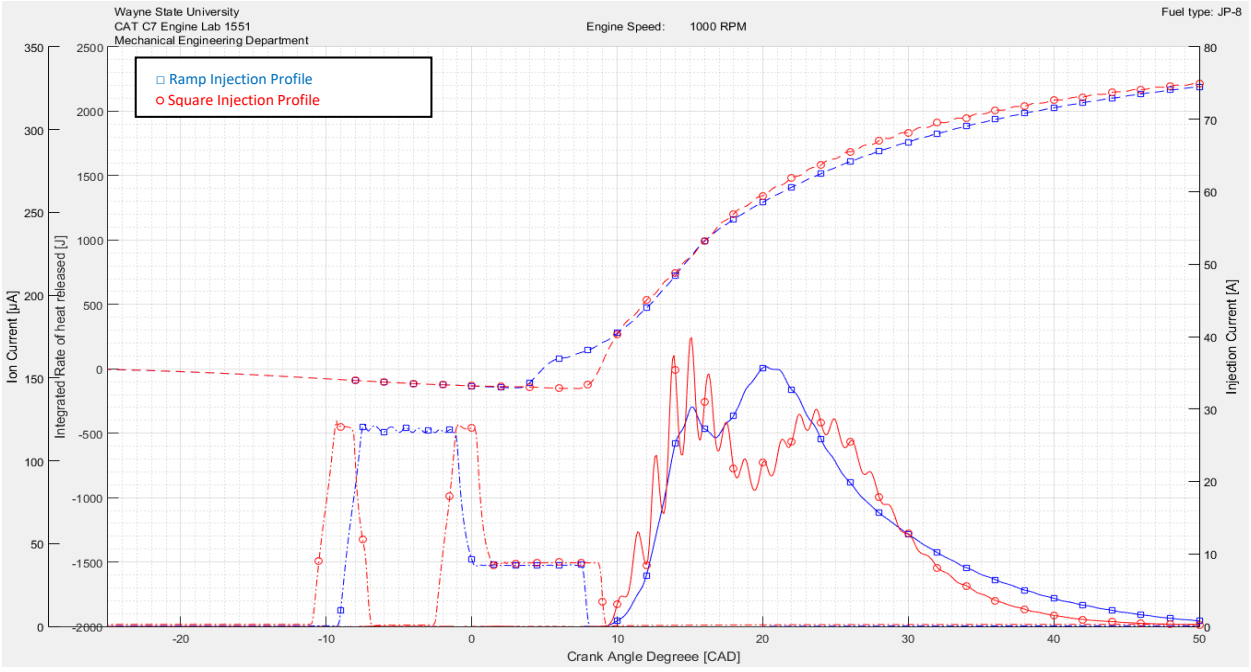

Speed:1000 RPM Load: 10 IMEP Injection Profile: Square Fuel: JP-8

Figure 4. 41 Effect of injection profile on the ion current signal and IRHR

Shown in figures (4.38), (4.39), (4.40) and (4.41) the effect of changing the injection rate shape on cylinder pressure, calculated mass averaged temperature, calculated rate of heat released and integrated rate of heat released respectively with respect to ion current signal and injector waveform common to all figures. As expected, more fuel is initially injected when single square injection is utilized compared to the single ramp injection allowing a larger fraction of the fuel injected to be premixed with air and result in a higher peak of premixed combustion shown in the RHR trace. Again ion current signal recorded two peaks when diffusion combustion is the dominant combustion mode.

SOFD at 1.9 bTDC and 2.9 aTDC for the ramp and square profiles respectively with injection delay period of 7.1 and 5.3 CAD. This emphasis square injection has a shorter injection delay.

It is also concluded that almost same amount of fuel is burnt to get the same load with different injection profiles. Mass of fuel is calculated by dividing the lower heating value of the fuel by the total energy calculated from the integrated rate of heat trace.

It is widely reported and evidenced by figure (4.40) that premixed combustion of the fuel cause a sharper rise in the in-cylinder pressure which in turns causes higher engine noise. Atzler et al [16] published a paper comparing the single ramp and square injection profiles and discussed the effect of the faster injection profile in increasing engine noise and PM emission while having the benefit of reducing engine-out NOx.

4.4.5 Results and observations

Using single injection event with the square rate profile results in higher peak of premixed combustion of the fuel across the whole range of loads for the experiment. Although premixed combustion is the dominant mode, it is expected for the diffusion combustion mode to be the dominant mode at higher engine loads. Increasing engine load resulted in increasing the peak of ion signal as higher temperatures are achieved. Figure (4.42) shows the effect of increasing engine load on the peak of ion current signal and also showing for the last load point (10 IMEP) it is easy to distinct between the combustion modes when premixed combustion peak starts decreasing accompanied with the increase in diffusion combustion peak however still premixed is the dominant combustion mode affecting the ion signal peak.

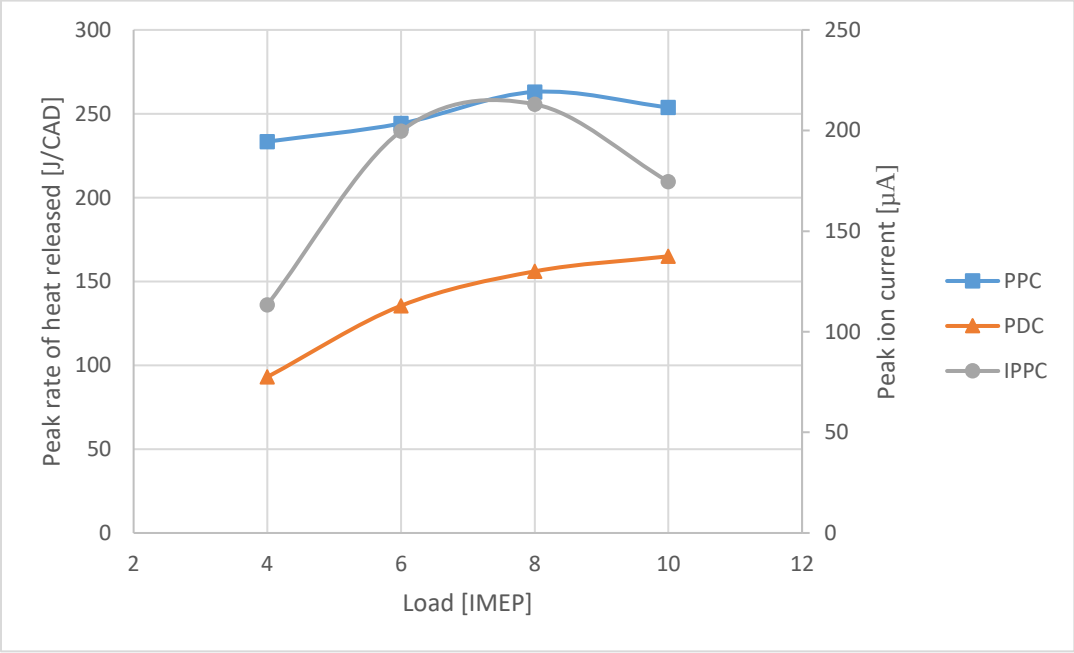

Figure 4. 42 Relation between RHR peaks and Ion current signal peak

Also concluded from the results stronger correlations between SOC-SOIC and SOFD-SOIC compared to the ramp injection profile.

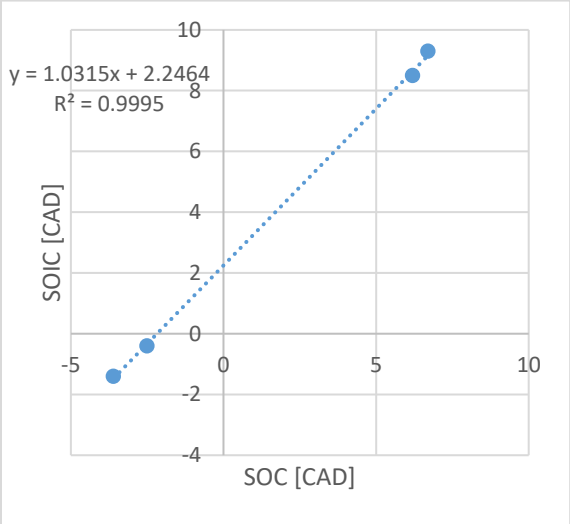

Figure 4. 43 SOC-SOIC correlation

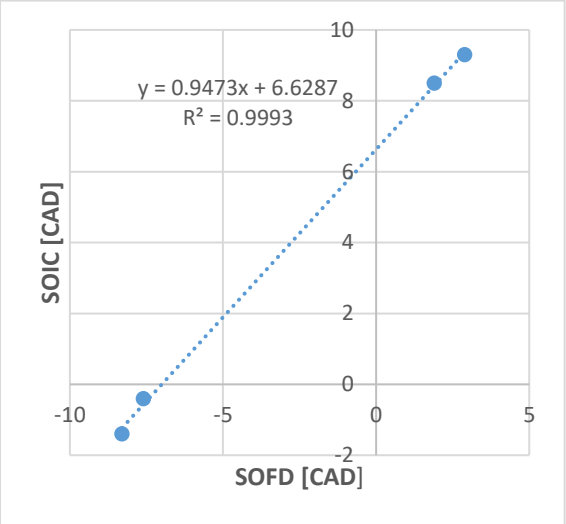

Figure 4. 44 SOFD-SOIC correlation

Shown in figures (4.43) and (4.44), linear trend lines fitted to the correlations having coefficient of determination, R^2 of 99.95% and 99.93% for SOC-SOIC and SOFD-SOIC correlations.

These correlations were studied for low and medium load conditions only with square injection profile.

4.5 Multiple injection events

4.5.1 HEUI injector operation

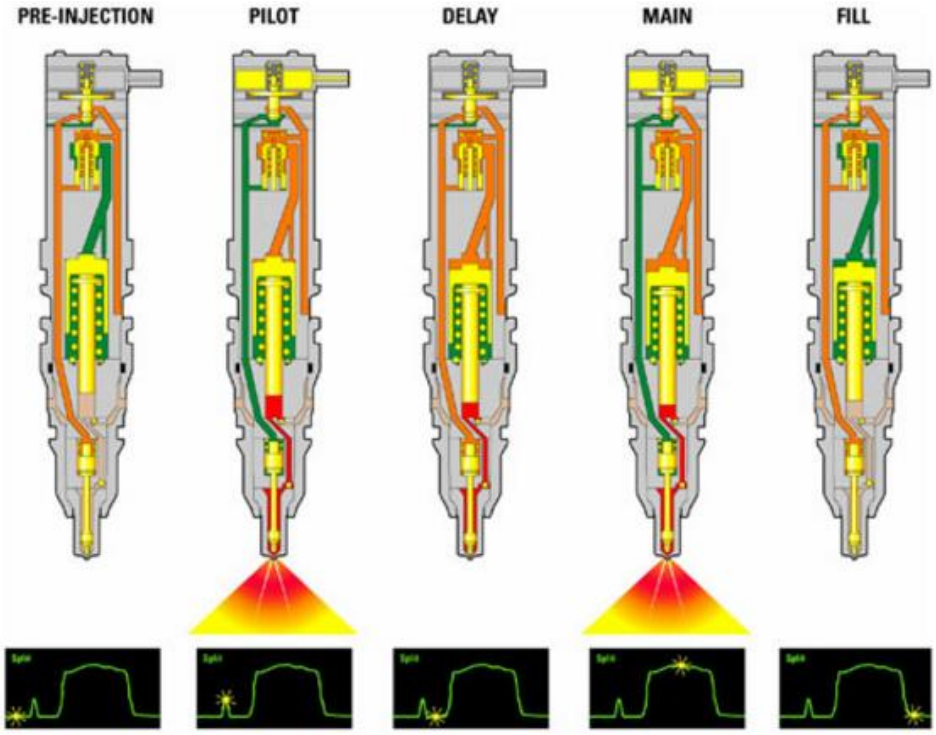

Figure 4. 45 HEUI-B Multiple injections events [13]

Multiple injection events can be obtained by changing the current waveforms timings and durations supplied to the injector solenoid. The HEUI-B injection systems are capable of achieving both pilot injection events preceding the main injection and post injection events as well as different injection rate shapes depending on the operating conditions and engine performance requirements.

Zhang [15] proved by experiments that pilot injection event can reduce the engine noise and engine out smoke at low load conditions since the pilot injection shortens the ignition delay of the main injection due to the temperature rise of the pilot combustion. Thus, when only utilizing the main injection event without pilot injection, the ignition delay of the fuel is longer and this gives more time for the fuel to mix with air resulting in a higher peak of premixed combustion which leads to higher engine noise.

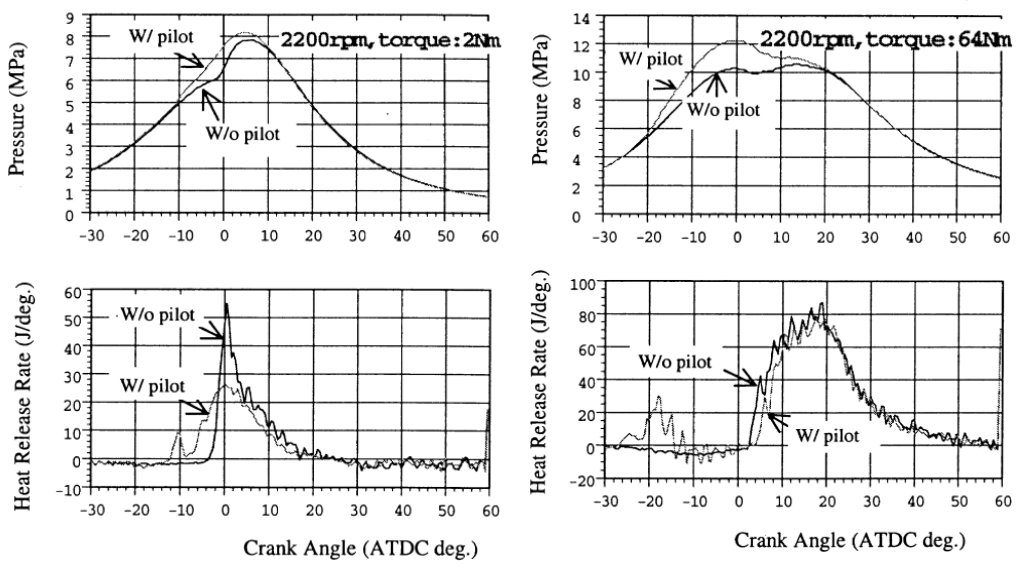

Figure 4. 46 Effect of pilot injection on the RHR [15]

However, at high engine load conditions pilot injection event had minimum effects on the injection delay period since combustion temperature is already high to shorten the ignition delay. Figure (4.46) shows the effect of pilot injection event on the combustion noise and engine out smoke.

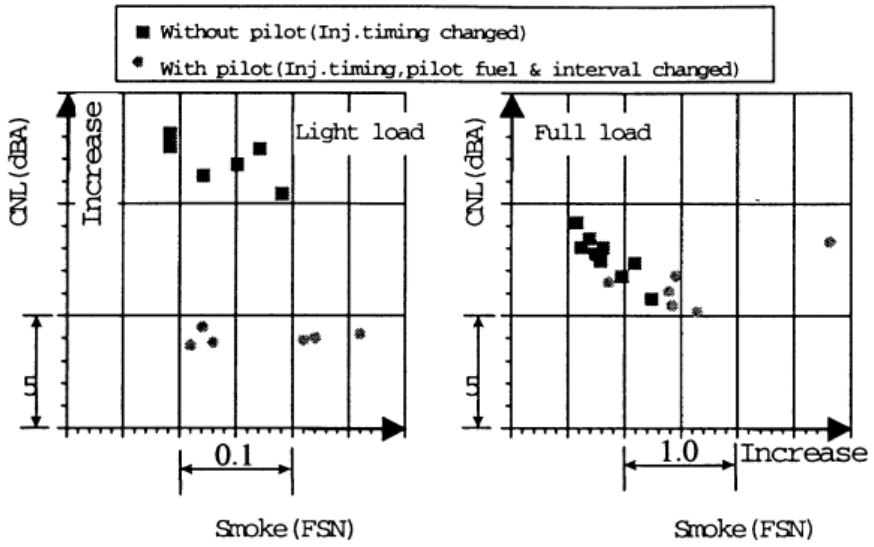

Figure 4. 47 Effect of pilot injection event on combustion noise and smoke [15]

Atzler et al [16] published a paper studying the difference between main injection event ramp rates with and without pilot injection.

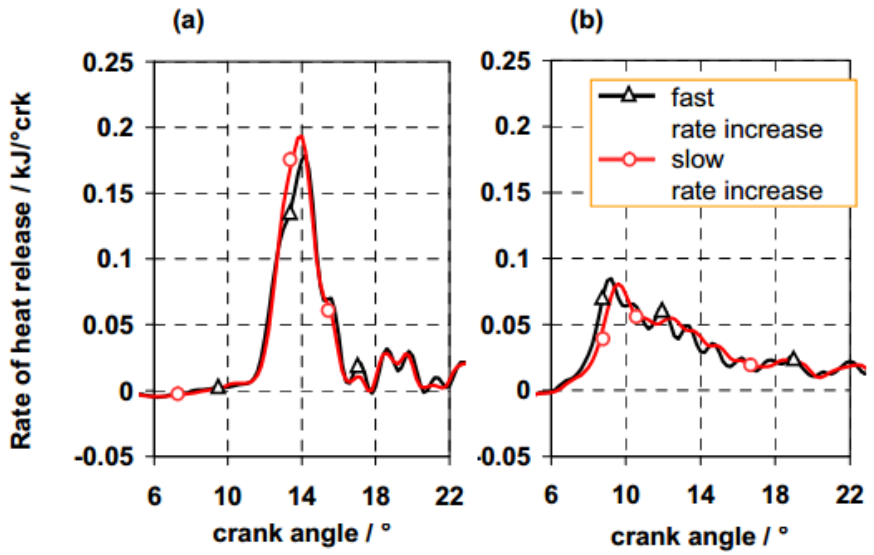

Figure 4. 48 Rate of heat released utilizing single main injection event (a) vs pilot and main injection events (b) using different injection rates [16]

In case of slow rate main injection event figure (4.48a), ignition delay is longer which gives a larger fracture of the fuel injected longer time to premix with the air resulting in a higher peak of

premixed combustion causing higher PM emissions compared to the fast rate “Square rate shape” [16].

Figure (4.48b) shows the comparison of rate of heat released trace of the main injection event while utilizing the pilot injection event. In this case, the use of pilot injection already shortened the ignition delay of the main charge. However, the fast rate causes larger amount of fuel is injected initially in the short ignition delay period compared to the slow rate resulting in higher PM emissions.

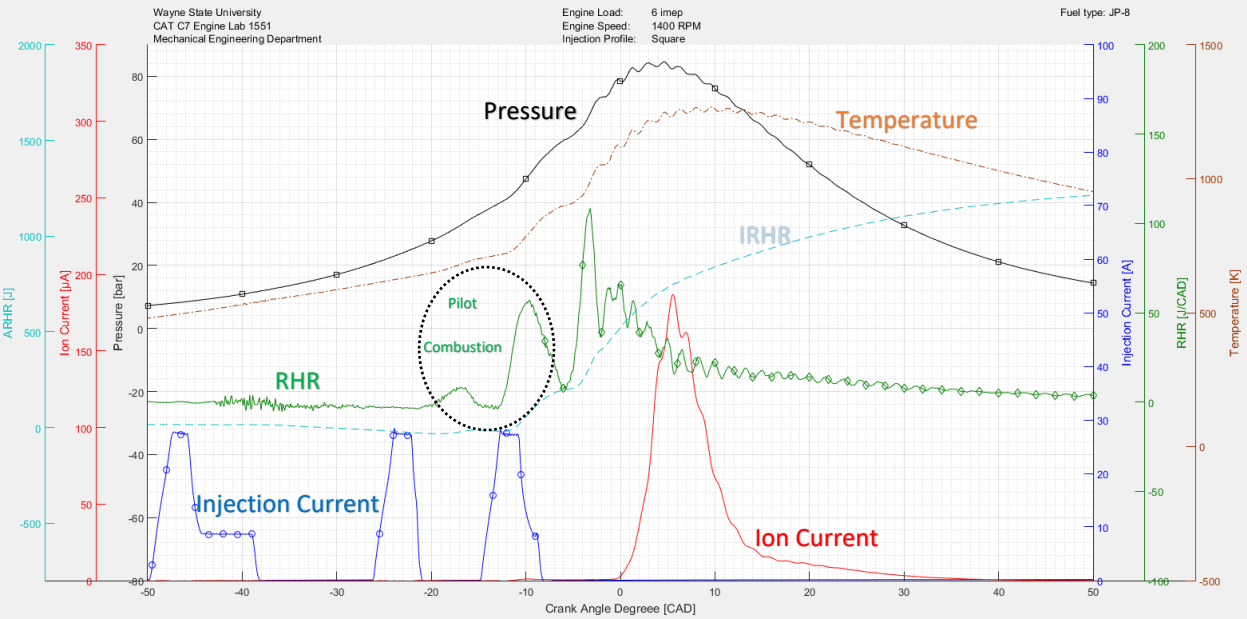

Figure 4. 49 Pilot injection ionization

Shown in figure (4.49) the effect of utilizing a pilot injection before the main injection event. Rate of heat released trace developed four distinct peaks. First two represent the premixed and diffusion combustion of the pilot injected fuel while the last two represent the premixed and diffusion combustion of the main injected fuel. Although pilot injected fuel was injected very early bTDC and should have had enough time for mixing and evaporation, the majority of the

pilot fuel burnt in a diffusion combustion regime. The diffusion combustion of the pilot fuel is the caused by the low in-cylinder temperature which in turns makes the fuel evaporation rate slower during the ignition delay period resulting in poor mixing quality in addition to not reaching the auto-ignition temperature. More likely, fewer particles of the pilot injected fuel contribute in the premixed combustion due to cylinder and piston wall wetting [16].

It is widely reported that pilot injections reduce the ignition delay of the main injection by raising the temperature which in turns reduces the premixed combustion mode effect of the main charge reducing engine noise and engine out smoke.

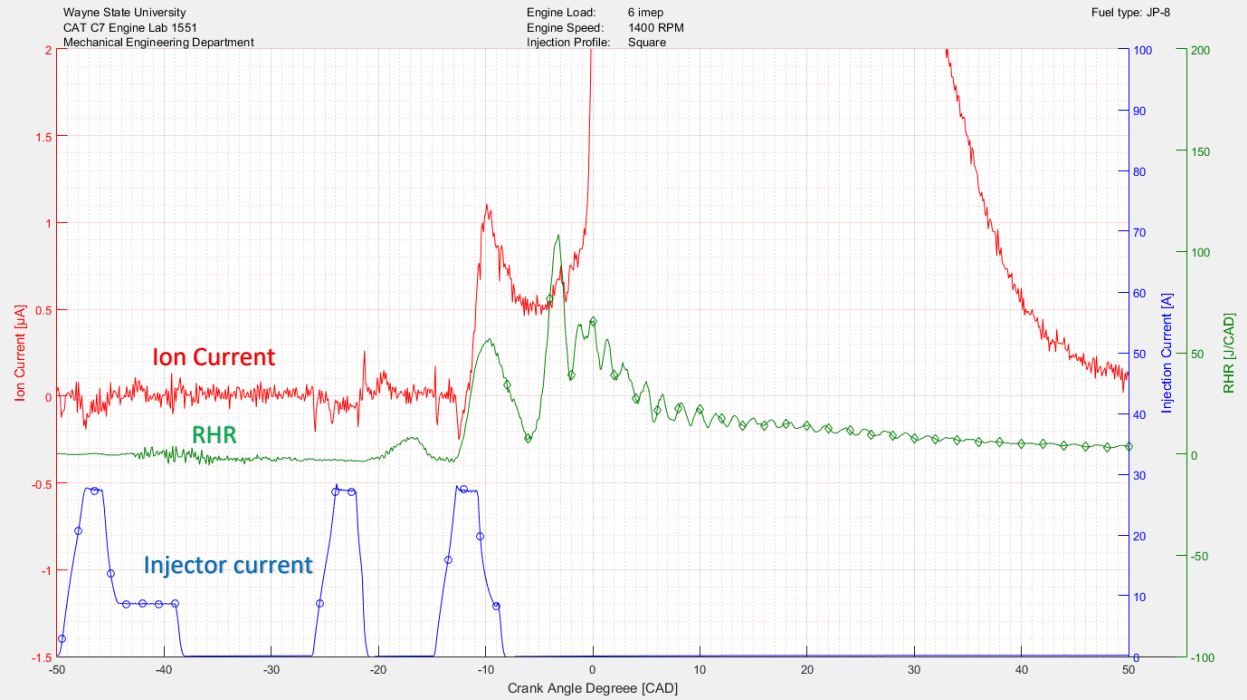

Figure 4. 50 Pilot injection_ zoomed ion signal

According to the injection profile and events map shown in figure (4.26), another experiment was conducted at higher engine speed medium load condition for the ECU to produce multiple injection events. With the engine running at 1400 rpm at 6 IMEP load it is noted that the ECU produces a pilot injection event preceding the square main injection. Shown in figure (4.50) the

effect of pilot injection on the ion current signal as 2 peaks are produced. The first peak is due to the diffusion combustion of the pilot injection since the majority of pilot injection burnt in a diffusion combustion mode. Second peak is due to the premixed combustion of the main injection.

Shown from figure (4.51) that pilot injection has very minimum effect on the peaks of the ion current signal taking into consideration that signals shown in this study was for an average of consecutive 100 cycles. It is believed that the pilot injection would have greater influences on the ion current signal and would show a distinct peak due to pilot injected fuel combustion at higher load conditions as higher in-cylinder temperature would be achieved.

By looking at the rate of heat release trace in figure (4.50), it was not possible to accurately specify the SOFD as studied in previous parts of this research since combustion of the pilot injection takes place very close to the main combustion event. It is very important to instrument the engine with a needle lift sensor to come up with the actual start of fuel delivery and validate the results obtained from the rate of heat released trace.

CHAPTER 5.0: CONCLUSIONS AND FUTURE WORK

5.1 Conclusions

1- Ion current signal was successfully demonstrated to be measured by an ion sensing probe in a compression ignition military engine equipped with a HEUI injection system running on JP-8 fuel

2- Correlations between start of ion current - start of fuel delivery and start of ion current – start of combustion were observed to follow a linear trend line.

3- Based on the correlations, ion current signal can be used for real time control of the C7 engine and calculate ignition delay to come up with the type of fuel burnt for multi fuel operation.

4- Utilizing square injection profile enhances the premixed combustion of the charge and higher amplitudes of ion current signal were observed compared to the slower ramp injection profile.

5.2 Recommendations for Future Work

1- The use of an injector instrumented with a needle lift sensor to determine the start of fuel delivery event and validate the characteristics of the injection system obtained from the rate of heat released analysis.

2- Enhancements to mechanical design of the ion sensor to be able to study the characteristics of the ion current signal utilizing multiple injection events at high load conditions.

REFERENCES

1. Randolph, A., "Methods of Processing Cylinder-Pressure Transducer Signals to Maximize Data Accuracy," SAE Technical Paper 900170, 1990, doi:10.4271/900170

2. Badawy, T., Henein, N., Bryzik, W., “Closed Loop Control Using Ion Current Signal in a Diesel Engine,” SAE Technical Paper 2011-01-2433, 2011.

3. Estefanous, F., Henein, N., “Multi Sensing Fuel Injector for Electronically Controlled Diesel Engines,” SAE Technical Paper 2011-01-0936, 2011.

4. Glavmo, M., Spadafora, P., and Bosch, R., “Closed Loop Start of Combustion Control Utilizing Ionization Sensing in a Diesel Engine,” SAE Technical Paper 1999-01-0549, 1999.

5. Kubach, H., Velji, A., Spicher, U., and Fischer, W.,“Ion Current Measurement in Diesel Engines,” SAE Technical Paper 2004-01-2922, 2004.

6. Henein, N., Badawy, T., Rai, N., Bryzik, W., “Ion Current, Combustion and Emission Characteristics in an Automotive Common Rail Diesel Engine,” ASME J. Eng. Gas Turb. Power, Vol 134, 042801-7

7. Estefanous, F., Badawy, T., Henein, N., “Cycle Resolved In-Cylinder NOx and Ion Current Measurements in a Diesel Engine,” SAE Technical Paper 2013-01-0555, 2013.

8. Rai, Nilesh. “Measurement and Analysis of Ion Current Signal in an Automotive Common Rail Diesel Engine,” Master’s Thesis, Wayne State University, 2010.

9. Peron, L., Charlet, A., Higelin, P., Moreau, B., Burq, J.F., “Limitations of Ionization Current Sensors and Comparison with Cylinder Pressure Sensors,” SAE Technical Paper 2000-01-2830, 2000.

10. Reinmann, R., Saitzkoff, A., Lassesson, B., Strandh, P., “Fuel and Additive Influence on the Ion Current”, SAE Paper 980161.

11. Glassey, S., Stockner, A., and Flinn, M., "HEUI - A New Direction for Diesel Engine Fuel Systems," SAE Technical Paper 930270, 1993, doi:10.4271/930270.

12. Hower, M., Mueller, R., Oehlerking, D., and Zielke, M., "The New Navistar T 444E Direct-injection Turbocharged Diesel Engine," SAE Technical Paper 930269, 1993, doi:10.4271/930269.
13. Coldren, D., Schuricht, S., and Smith, R., "Hydraulic Electronic Unit Injector with Rate Shaping Capability," SAE Technical Paper 2003-01-1384, 2003, doi:10.4271/2003-01-1384.

14. Tanabe, K., Kohketsu, S., and Nakayama, S., "Effect of Fuel Injection Rate Control on Reduction of Emissions and Fuel Consumption in a Heavy Duty DI Diesel Engine," SAE Technical Paper 2005-01-0907, 2005, doi:10.4271/2005-01-0907.

15. Zhang, L., "A Study of Pilot Injection in a DI Diesel Engine," SAE Technical Paper 1999-01-3493, 1999, doi:10.4271/1999-01-3493.

16. Atzler, F., Kastner, O., Rotondi, R., and Weigand, A., "Multiple injection and rate shaping Part 1: Emissions reduction in passenger car Diesel engines," SAE Technical Paper 2009-24-0004, 2009, doi:10.4271/2009-24-0004.

17. Stockner, A., Flinn, M., and Camplin, F., "Development of the HEUI Fuel System-Integration of Design, Simulation, Test, and Manufacturing," SAE Technical Paper 930271, 1993, doi:10.4271/930271.

18. Henein, N. and Bolt, J., "Correlation of Air Charge Temperature and Ignition Delay for Several Fuels in a Diesel Engine," SAE Technical Paper 690252, 1969, doi:10.4271/690252.

19. Lee, J., Jeon, J., Park, J., and Bae, C., "Effect of Multiple Injection Strategies on Emission and Combustion Characteristics in a Single Cylinder Direct-Injection Optical Engine," SAE Technical Paper 2009-01-1354, 2009, doi:10.4271/2009-01-1354.

20. Badwy T., “ionization in Diesel Combustion for On-Board Diagnostics and Engine Control” PhD Dissertation, Wayne State University, 2013.

21. Larsson, M., Denbratt, I., Koopmans, L., “Ion Current Sensing in an Optical HCCI Engine with Negative Valve Overlap,” SAE Technical Paper 2007 01-0009, 2007.

ABSTRACT

COMBUSTION PHASING THROUGH COMBUSTION IONIZATION IN A CATERPILLAR C7 COMPRESSION IGNITION ENGINE

by

Kamal Assaad

September 2016

Advisor: Dr. Naeim Henein

Major: Mechanical Engineering

Degree: Master of Science

To achieve the goals of best fuel economy, peak power and low soot emissions in military engines it is necessary to control the combustion process. An in-cylinder combustion sensor is required to achieve the goals of controlling the combustion process. Over the last four decades, in-cylinder pressure transducers and ion current sensors have been available for research and development. Most of the effort has focused on the pressure transducer, however up till now a pressure transducer suitable for use in production engines has not been developed yet, because of cost and durability concerns. This work presents the analysis of experimental data proving the relationship between the start of combustion and ionization event conducted on a military compression ignition engine equipped with hydraulic electronically controlled injection system.

AUTOBIOGRAPHICAL STATEMENT

Kamal Assaad graduated from Arab Academy of Science and Technology and Maritime Transport (AASTMT) in 2012 with a Bachelor of Science in Mechatronics Engineering. His professional career began in Feb 2012 working at El-Kamal Industrial Company

Pursuing his master's degree in mechanical engineering, Kamal joined Wayne State university in 2014 conducting research related to combustion ionization in the CAR (Center for Automotive Research) under supervision of Dr. Naeim Henein. In 2015 he joined Detroit Engineered Products as an engineering intern which turned into a full time employment in 2016 as an IC project engineer.